NAZARBAYEV UNIVERSITY

School of Engineering and Digital Sciences

Bachelor of Engineering in

Mechanical and Aerospace Engineering

Designing and Manufacturing of a Liquid Piston Rotary Engine, and Comparison of Performance with Wankel's Rotary

(Final Capstone Project Report)

by

Adil Olzhabayev, Ulan Kushtibayev, Meirambek Tassybay

Lead Supervisor: Prof. Desmond Adair

Co-Supervisor: Prof. Basman Elhadidi

May, 2025

Declaration

We, Adil Olzhabayev, Ulan Kushtibayev, Meirambek Tassybay, hereby declare that “Designing and Manufacturing of a Liquid Piston Rotary Engine, and Comparison of Performance with Wankel's Rotary ” project report is the product of our own project work except for quotations and citations which have been duly acknowledged. We declare that it has not been previously or concurrently submitted for any other degree at Nazarbayev University or elsewhere.

Signature:
Adil Olzhabayev
Ulan Kushtibayev
Meirambek Tassybay

Name: Adil Olzhabayev, Ulan Kushtibayev, Meirambek Tassybay
Date: November 28, 2024

Acknowledgments

Sincere gratitude to:

Our Capstone project supervisor professor Desmond Adair for his guidance in this project and answering our questions at any time we needed.

Our Co-Supervisor professor Basman Elhadidi for his guidance and support throughout this project.

MAE Department of Nazarbayev University for providing the necessary equipment and materials to accomplish the project's target.

Our family and friends for their invaluable support.

Abstract

Rotary engines, known for their high power-to-weight ratio, are offered as a compelling alternative to conventional engines. However, major drawbacks such as thermal inefficiency, high emissions, and limited durability are also exhibited. In this Capstone project, the Wankel engine, a classic rotary architecture, is compared with the LiquidPiston engine, a modern alternative employing the High-Efficiency Hybrid Cycle to address the Wankel's limitations. The goal of this study was to assess whether modern cycle innovations can yield measurable improvements in efficiency and durability, and to determine the applicability of rapid prototyping for concept validation. Detailed 3D CAD models were developed and static simulations were conducted, but experimental tests using 3D-printed prototypes revealed critical assembly and material constraints that prevented rotor motion under compressor load. 3D modeling of both the engines was conducted, followed by computational evaluation of major performance factors such as thermal efficiency, output power, emission calculations, and structural lifespan. Experimental validations were then undertaken. Preliminary literature and simulation data suggest that the LiquidPiston engine is better than the Wankel design on all the metrics studied. A thorough comparative evaluation has been established to fill the research literature gap on the performance comparison of rotary engines.

Contents

Introduction

Rotary engines due to their size, smooth operation and high power-to-weight ratio, which make them advantageous for automotive and aviation applications where space efficiency and lightweight design are critical , have been the center of interest for engineers and researchers for decades [1], [4]. Unlike traditional reciprocating engines, rotary engines rely on the rotational motion of a rotor within an epitrochoidal chamber, offering smoother operation with fewer moving parts [8]. This simplicity of the rotary engines makes it appealing for applications requiring high reliability and reduced maintenance [1], [7].

1.1. Historical Context

Felix Wankel invented the most widely recognized rotary engine, named after him The Wankel engine, in the 1950s [8]. It quickly gained attention for its innovative design that replaced traditional pistons with a single triangular rotor. The compact design of the engine provided a unique advantage over conventional engines, having a higher power-to-weight ratio with smoother performance [4]. All that made it ideal for niche applications such as the Mazda RX-series sports cars, which became an icon of automotive innovation, and also for usage in unmanned aerial vehicles (UAVs) where space and weight are crucial criteria [8].

However, despite having success in specific domains, Wankel Rotary engine had its challenges. Apex seals, which are crucial for maintaining compression, suffer from leakage and excessive wear [7]. In addition, due to its combustion chamber being unconventional, it results in incomplete combustion and high thermal losses, which leads to poor efficiency and high emissions level[4], [7]. In light of modern environmental regulations, its limitations restricted more broader adoption of engine [10]. The engine’s decline in popularity shows the need for advancements to address its technical challenges [3].

1.2. Modern Developments in Rotary Engines

In past decade, the LiquidPiston rotary engine, developed by LiquidPiston, Inc., has developed as promising alternative to Wankel's traditional rotary engine, its new design incorporates the High-Efficiency Hybrid Cycle (HEHC), which combines elements of the Otto, Diesel and Atkinson cycles [5]. Key opportunities HEHC cycle has that overcome drawbacks of Wankel engines are enhanced thermal efficiency, reduced emissions and improved reliability [6]. The LiquidPiston engine achieves these improvements by innovative features in design, which is like inverted Wankel engine, resulting in effective thermal management systems alongside better sealing technology [5], [6]. Unlike traditional rotary engines, the LiquidPiston engine minimizes its reliance on apex seals, thus reducing wear and leakage [6], [9]. Engine's HEHC cycle is tailored to maximize its efficiency on heat into mechanical work conversion, addressing the inefficiency of old rotary engines [5]. These advancements make the LiquidPiston engine well suited for applications in modern day with environmental regulations, where high performance is essential, such as drones, hybrid vehicles and portable generators.

1.3. Research Gap

Despite the LiquidPiston engine having all these innovations that are solutions for drawbacks of Wankel engine, comparative analysis on similar operating conditions are underexplored. While there are individual studies made to evaluate thermal efficiency, emissions and durability of engines, head to head comparison is lacking. Such a comparison is crucial in order to understand the practical advantages of LiquidPiston engine design over Wankel engine, and to identify its potential application in automotive and aerospace industries.

1.4. Project Objectives

This Capstone project's objective is to fill this gap by evaluating and comparing the performance of Wankel and LiquidPiston engines, in different aspects. The study will focus on key parameters such as:

- Thermal efficiency
- Power output
- Durability under operating conditions

By designing, modeling and simulation both engines and manufacturing for physical tests, both from plastic for air compressor tests and for metal manufacturing. Project aims to determine their relative strengths and weaknesses. The findings will give insights into the application opportunities of these engines in various industries and offer recommendations for future advancements in rotary engine design.

1.5. Scope of the Report

This report will begin with a thorough literature review that will provide background information on rotary engine technology, including the evolution of the Wankel and LiquidPiston engines over time and their latest developments. The design, modeling, and simulation methods used to evaluate engine performance will be discussed in detail in the methodology section. The simulation results will then be shown in the results section, followed by a discussion section to identify important parallels and insights. The conclusion will conclude by summarizing the results, considering their implications, and identifying possible directions for further research.

2. Literature Review

2.1. Background of Rotary Engines

Wankel Rotary engine, replaced conventional pistons with a rotating triangular rotor, well known for its compact size in relation with conventional engines and high power-to-weight ratio. It was invented by Felix Wankel in the 1950s, was used in Mazda RX series and in Unmanned Aerial Vehicles [8].

Wankel's rotary engine, despite being compact and powerful, has significant drawbacks in thermal efficiency, resulting from its elongated combustion chamber. Geometry of the chamber leads to uneven heat distribution, which leads to incomplete combustion, which leads to significant thermal losses [4], [6]. Also problems with apex seals, that is for maintaining compression, sufferers from wear and leakage, that leads to reduced fuel efficiency and increases emissions of hydrocarbons (HC), carbon monoxide (CO) and nitrogen oxides (NOx), that led to limited usage under environmental regulations [7]. [10].

Researchers have explored various improvements that could be done in Wankel engine design. For instance, Eiermann et al. (1990) focused on enhancing engine's efficiency for lightweight applications, though the combustion chamber shape remains a challenge [1]. Finkelberg et al. (2019) showed approaches to optimize the combustion process while Yang et al. (2023) solved apex seal leakage and significant change in emissions and inefficiencies [2], [7].

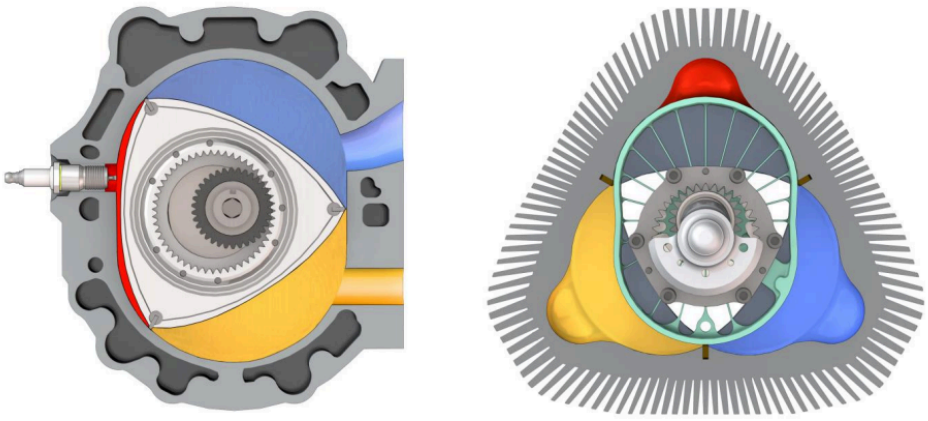

Figure 1. Comparison of Wankel engine and LiquidPiston Engine [11]

The LiquidPiston engine was developed as a modern alternative to the Wankel Engine. THe LiquidPiston engine uses High-Efficiency Hybrid Cycle (HEHC), which combines properties of Otto, Diesel and Atkinson cycles to optimize fuel conversion efficiency and emission decrease [5], [6]. The biggest change is design that looks like an inverted Wankel engine, with an oval rotor in triangular housing, changes combustion chamber geometry and reduces reliance on apex seals, resulting in less leakage and enhanced durability. That change in combustion chamber geometry led to more complete combustion, resulting in lower emission [10].

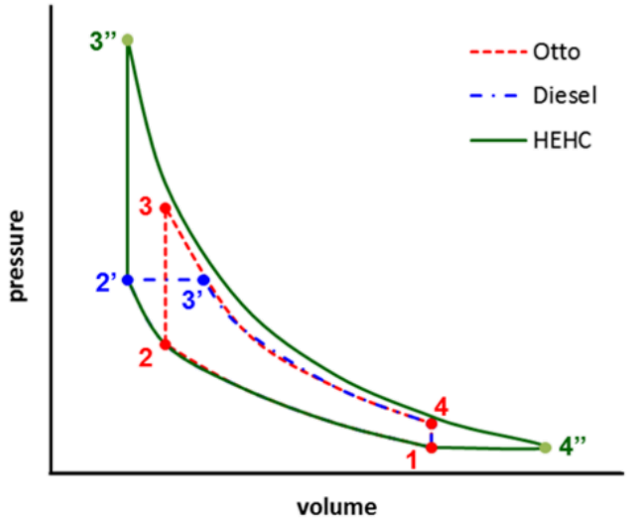

Figure 2. HEHC cycle [5]

Another advantage of the LiquidPiston engine is flexibility in fuel choice, an engine capable of operating on renewable fuels such as biodiesel and methanol, making it a good option for hybrid vehicles and portable power systems [6], [9]. Nickerson et al.(2018) demonstrated that the LiquidPiston engine can achieve 45% brake thermal efficiency, significantly better than typical 20% to 30% thermal efficiency of Wankel's engine [5].

2.2. Performance Comparative Analysis of Rotary Engines

Thermal efficiency

Wankel Engine demonstrates elongated combustion chamber geometry, resulting in incomplete combustion. And additional thermal losses due to apex seal leakage [4], [7]. According to the research, reported thermal efficiency range between 20% and 30% [1]. On

the other hand, LiquidPiston Engine uses HEHC cycle, which leads to higher thermal efficiency and minimizes heat loss [5], [6]. LiquidPiston Engine's reported thermal efficiency reached up to 45% [6]. Looking at the results it shows that thermal efficiency of LiquidPiston is almost 2 times of Wankel engine.

Power output

Wankel Engine's experimental data shows a single rotor Wankel engine can achieve output of 26 kW at 6000 RPM, with twin-rotor configurations doubling capacity twice at higher RPMs [1]. On the other hand, LiquidPiston Engine's specific power output values are reported to be 1.5 higher than traditional engines of similar sizes [5]. Both engines offer competitive power-to-weight ratios.

TABLE 3 - Main features of the LCCR family of engines

ENGINE FEATURE	Single Rotor Engine LCCR 400S	Twin Rotor Engine LCCR 800T
Performance	26 kw / 6000 RPM	52 kw / 6000RPM
Displacement	407cc / Rev	816cc / Rev
Dry Weight	26 kg - 57 lbs	36 kg - 79 lbs
Dimensions: mm inch	400L x 268H x 303W 16L x 11H x 12W	500L x 268H x 303W 20L x 11H x 12W
• Liquid Cooling System - Thermostat Control • Basic Version - Gasoline, carburated or low pressure injection system • Advanced Version - Turbine fuel and diesel fuel with high pressure injection system • Ignition System - Single or double spark plug system with electronic pick up sensor • Engine installation - Horizontal or vertical - any attitude • Lubrication system - Total loss system; Metering pump; no oil sump		

Figure 3. Table featuring performance results [1]

Emissions

Wankel Engine's elevated levels of carbon monoxide (CO) and hydrocarbons (HC) due to incomplete combustion. Also, the high surface-to-volume ratio of the combustion chamber exacerbates nitrogen oxides (NOx) emissions under high temperature [2], [4].

On the other hand, LiquidPiston Engine HEHC cycle minimizes unburned hydrocarbons and reduces particulate matter (PM) and NOx emissions, enabling it to meet environmental standards [5], [10]. Overall, the LiquidPiston emissions level is much lower in comparison to Wankel engines.

Durability

Wankel Engine shows results in thermal stress that degrades materials integrity due to apex seal wear combined with uneven heat distribution [3], [7]. On the other hand, LiquidPiston Engine's enhanced sealing technologies reduce seal wear. In the LiquidPiston engine thermal management mitigates materials stress degradation, ensuring stable performance under high-load conditions [5], [6]. Overall, improved thermal performance and advancement in sealing parts results in favor of LiquidPiston engine, which significantly reduces maintenance requirement compared to Wankel Engine [6].

2.3. Summary of Comparative Analysis

Table 1. Performance metrics of engines

Metric	Wankel Engine	LiquidPiston Engine	Advantage
Thermal Efficiency	20%-30%	Up to 45%	LiquidPiston
Power Output	High power-to-weight ratio	In addition to high power-to-weight ratio, compatibility with better fuel efficiency	LiquidPiston
Emissions	High level of CO,HC and NOx	Low level of CO,HC and NOx	LiquidPiston
Durability	Prone to apex seal wear and thermal stress	Better sealing and thermal management	LiquidPiston

Results of comparisons based on literature review shows that LiquidPiston is better compared to Wankel engine.

2.4. Research Gaps and Future Directions

Despite significant advancements in the technological side, several research gaps remain. That one being lack of direct comparison of these engines at standard conditions. Future should concentrate on long-term durability. Literature review indicated potential opportunities for improved performance of Liquid Piston, but it needs to provide tests at high-load conditions to mitigate wear problems. The second aspect to concentrate on is integration of renewable energy. Although LiquidPistons are available to handle hydrogen, hydrogen use tendencies typically indicate fuel cell usage to generate electricity, and not burning. Therefore, testing on other biofuels should be conducted, to check the efficiency.

3. Methodology

3.1. Design and 3D Modeling for Simulations

The engine geometry and principal operating conditions were chosen both to take advantage of existing rotary engine practice as well as the capabilities of our test facility. The 239.75 mm diameter of the outer casing and 74.59 mm of its width come straight from Yamamoto's ideal Wankel geometry with its 500 cm^3 swept volume per chamber and 10 : 1 compression ratio suitable for delivering maximum shaft power near 30 kW at intermediate-speed operation [8], [5]. The 30 mm port bores were selected for delivering an intake volumetric rate of order 1.5 m^3/min capability for 4 500 rpm, consistent with automotive-port-to-chamber area ratios and supporting efficient gas exchange [3]. For the LiquidPiston engine, use of approximately 350 cm^3 swept volume with 9 : 1 compression ratio conformed to manufacturer specifications for the XMv3 platform [9].

All of the simulation domains are given the same aluminum 6061-T6 material characteristics (ρ = 2700 kg/m^3, k = 167 W/m·K, c□ = 896 J/kg·K) for modeling the intended metallic components. The combustion chamber is filled with a stoichiometric air–fuel mixture at 25 °C and 101.3 kPa [10], leading to maximum mean effective pressures of 8–10 bar with adiabatic flame temperatures of approximately 2000 K. Conjugate heat transfer analysis is used with uniform wall heat flux of 5 kW/m^2, as applied in measured hot losses from the XMv3 engine [15]. Sub-millimeter fillets as well as non-critical surface features were stripped from the CAD for enhancing mesh quality as well as for curtailing solution time, with all sealing as well as port features influencing flow as well as pressure dynamics being maintained.

Designing and 3D modeling of accurate 3D models is crucial for this project to have successful and profound results. This will mainly enable better simulation results and availability of manufacturing for physical tests. The rest of the design and drawing you can find in Appendix A

Parallel Trochoid Curve in Rotary Engine Design

The inner surface specified in the design of a rotary engine rotor housing follows a parallel trochoid curve. This is a modification of the standard trochoid curve, which mainly comes from the action of a point-on-a -circle rolling along a straight line. The point, however, appears on the surface of the parallel trochoid; the curve is offset outward by a fixed distance and hence produces a parallel path to the original trochoid.

This is for the case so that the apex seal which seals the compression inside the engine maintains itself with the touch of the inner surface of the housing during the complete

rotation of the rotor. The level of the parallel offset is, therefore, the key to the efficiency and durability of the engine; for destruction is reduced, as well as for sealing purposes.

The parallel trochoid equation curve (Figure 4) is given by the equations as follows:

$$x = e * cos(\alpha) + R * cos(\alpha/3) + a * cos(\alpha/3 + \varphi) \quad (1.1)$$

$$y = e * sin(\alpha) + R * sin(\alpha/3) + a * sin(\alpha/3 + \varphi) \quad (1.2)$$

Where:

R: is the radius of the rolling circle

a: is the constant offset

α: angle of rotation of revolving circle B around circle A

φ: is the angle of oscillation of the apex seal

The use of this curve in the rotor housing design ensures that the rotor maintains smooth motion within the housing, with minimal friction and optimal sealing during engine operation.

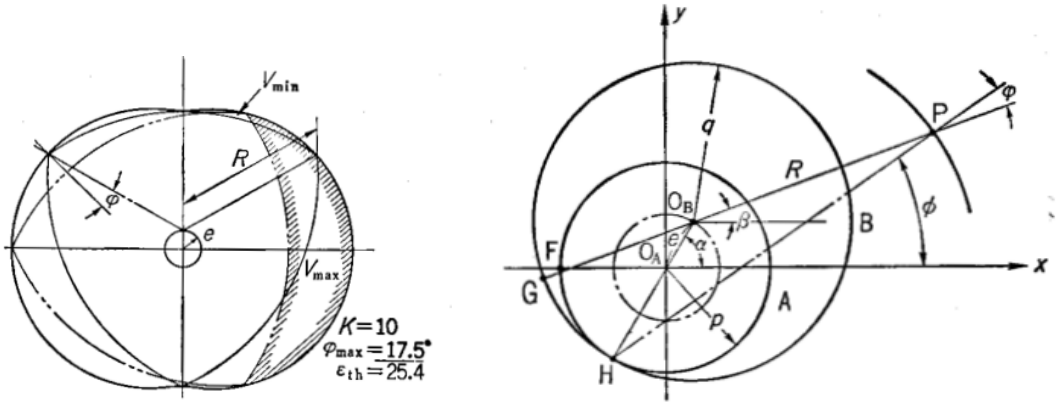

Figure 4. Trochoid constant and trochoid configuration [8]

Table 2. Practical application of the dimensions for Wankel rotary engine by Kenichi Yamamoto [8]

V_H(cc)	e(mm)	R(mm)	a(mm)	h(mm)	K	φ_{max}(degree)
60	7.6	47	0.5	32	6.18	29.0
129	9.5	65	0.5	40	6.85	26.0
150	10.5	66	1	41	6.28	28.5

Where V_H is the stroke volume.

Wankel Engine:

Table 3. Wankel Engine design summary

	Simulation Model	**Printing Model**
Purpose	Computational analysis of performance using computational simulations.	Physical prototyping and testing with an air compressor.
Key Features	Highly detailed housing and Rotor geometry.	Simplified geometry taking account of usage with compressed air. Considering proper intake and exodus for air.
Status	Finished but not yet simulated fully	Finalized but not yet printed

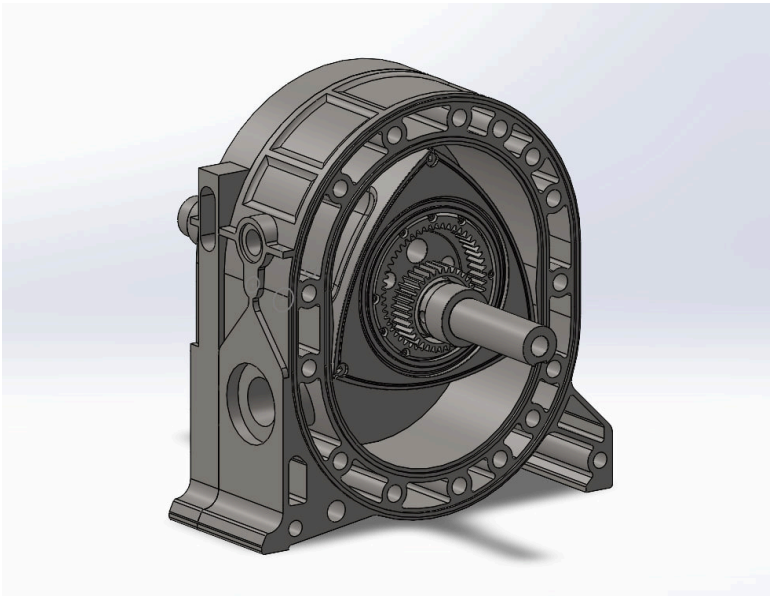

Figure 5. Wankel Engine for Simulations

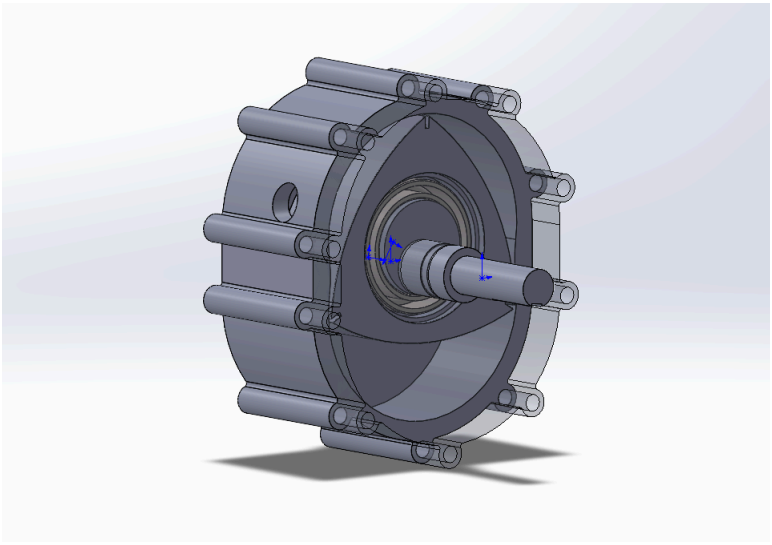

Figure 6. Wankel Engine simplified for simulation

LiquidPiston Engine:

Table 4. Liquid Piston Engine design summary

	Simulation Model	**Printing Model**
Purpose	Computational analysis of performance using computational simulations.	Physical prototyping and testing with an air compressor.
Key Features	Highly detailed housing and Rotor geometry. Making sure possibility for further manufacturing considering ability of technologies on hand.	Simplified geometry taking account of usage with compressed air. Considering proper intake and exodus for air.
Status	Under development, due to lack of data on factual dimensions.	Finished, might need some adjustments. Not yet printed

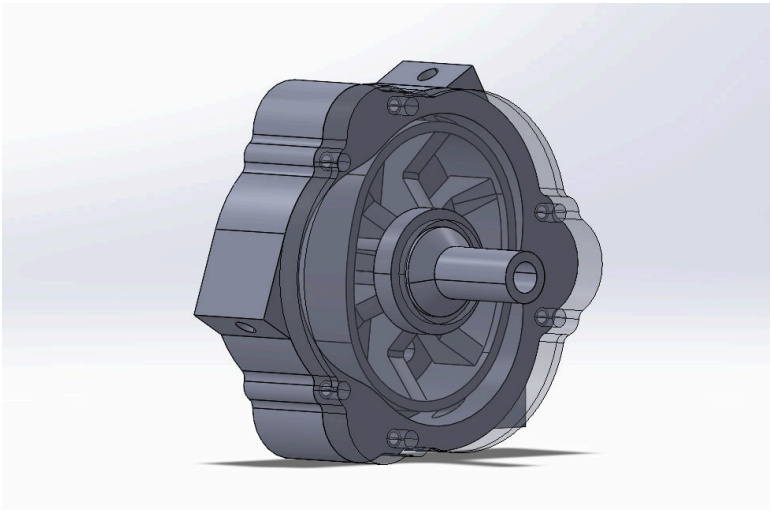

Figure 7. LiquidPiston Engine simplified for simulation

3.2. Design and 3D Modeling for Experiment

Design parameters, such as chamber volume, port dimensions, and the thickness of the walls, were determined to meet a 0.3 L swept volume and fit within the 225×225 mm build envelope of the Bambu Lab X1E and survive compressor performance at 5 atm. The 0.3 L of swept volume was selected to match the compressor's nominal displacement and to keep pressure and temperature transients within the range measurable by our sensors without subjecting the components to excessive cyclical stress that can lead to component failure. The 350 cm^3 swept volume, the 6.00 mm port bores, and the radius of the parallel-trochoid profile of 65.35 mm were determined to match the compressor's flow rate at constant pressure at 5 atm. Wall thickness of 10.00 mm at the base and 3.00 mm at the cap were a compromise between structural stability under cyclical 5 atm pressure and minimizing mass to keep the requirements for torque low.

All features essential to instrumentation and sealing were included in the simulation CAD models and translated to the experimental geometries. M5 connection bosses were included along the chamber circumference to provide space for pressure transducer and thermocouple well placement at intake and mid-chamber positions. All essential dimensions are held to a ±0.2 mm tolerance, as found through experimentation on the Bambu Lab X1E for FDM printing, to reduce leakage during high-pressure compressor testing.

The rotor shape retains the 51.21 mm apex path radius and 8.50 mm tip thickness and provides eight relief slots to minimize inertia and provide rapid equalization of pressure within the cyclical compressor environment. A 10.40 mm threaded section and 19.85 mm journal diameter stepped shaft provides standard compressor coupling interfacing capability; 13.00 mm knurled retaining nut facilitates assembly during testing.

The intake port features an off-the-shelf bicycle nipple adapter for a tough, threaded connection to pressure tubing that utilizes its precise M5-compatible threading. The rotor is supported on the shaft by precision deep-groove ball bearings 6004Z, and smaller 6001Z bearings hold the shaft in the housing to provide low-friction rotation and positional precision under dynamic load cycling.

Final experimental models were also exported as high-resolution STL files (tolerance of ±0.02 mm) and only contain the features relevant for the pressure testing, without ornamental fillets or supports. All the drawings for reference are given in the Appendix A.

The figure 8 depicts isometric assembled views of the experimental prototypes without caps for the housing.

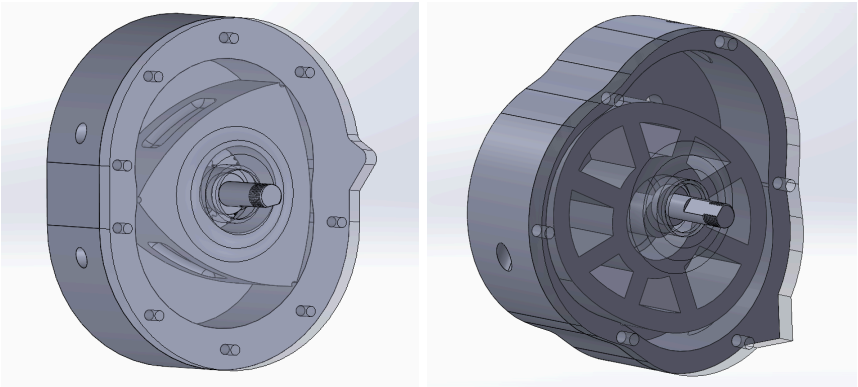

Figure 8. Engine models for 3D printing

Graphite as a lubricant

Graphite lubricant powders are found to reduce friction and enhance wear resistance at high temperatures, as shown by previous studies. For instance, the journal Tribology International released a report on how graphite lubricants decreased the coefficient of friction and improved wear resistance in high-temperature conditions, indicating that they are being used in extreme conditions [12].

In addition, the lubrication effect of graphite is influenced by conditions in the environment, which include humidity. A Nature Communications study found that the lubrication effect of graphite has to do with humidity--water held in molecular form forms a layer ongraphite which facilitates passivation and lubrication of defects [13]. This capability to accommodate humidity makes graphite an effective lubricator under ever-changing conditions.

Compatibility with 3D-printed materials has also been explored with the case of ABS composites. The Materials study examined the tribological performance of graphite powder-filled ABS composites and determined that adding graphite enhanced the material's friction and wear performance, making them valuable for mechanical components 3D-printed [14].

In short, the large body of literature attests to the applicability of graphite powder as the lubricant for 3D-printed rotary engine models. Its low wear rate, good wear resistance, environmental flexibility, and conformity to 3D-printed materials render it the best fit for increasing the performance and lifespan of such models.

3.3. Tools and Software

For designing, 3D modeling and further manufacturing advanced tools and software are used.

Software usage:

- **Solidworks:** Used fo creating precise 3D CAD models of both engines
- **Ansys:** Planned for comprehensive computational analysis of the engines
    - Thermal Analysis: Evaluating heat distribution
    - Structural Analysis: Evaluating stress and deformation in critical components
    - Fluid Dynamics: Simulating air-fuel flow, combustion and exhaust behavior
- **Bambu studio:** Used as slicing software to prepare for 3D printing by creating G-code.
- **Arduino IDE:** Developing and uploading firmware for the Arduino-based RPM measurement system used during compressor tests.

Manufacturing Tools:

- **BambuLab 1XE 3D printer:** Used for manufacturing prototypes for testing from plastic.
- **5 or 3 axis CNC machine:** Planned to be used for manufacturing LiquidPiston Engine from solid metal blocks

3.4. Instrumentation

List of materials:

- PETG filament (1 kg spool, Bambu Lab)
- Graphite leads
- Graphite powder lubricant (self-made from leads)
- 200-grit sandpaper
- Bicycle tire Presta valve
- Adapter for compressor-to-housing connection
- Akfix two-component glue
- M5 bolts and nuts for prototype assembly
- M10 nuts used as interchangeable test weights for shafts
- 3D-printed disk with integrated M10-threads for nuts, used for tachometer testing
- Arduino Uno R3 microcontroller
- Slotted optical tachometer sensor module (IR emitter/detector board)

In preparation for testing with the compressor, PETG filament was chosen to produce both the prototype housing and rotor to provide enough mechanical integrity and dimensional accuracy. Hand-extracted graphite leads from standard HB pencils were used to form the apex seals, and homemade graphite powder ensured regular lubrication between the housing surfaces and the seals. The finish and tolerance of the FDM-printed components were smoothed with 200-grit sandpaper to provide accurate seal engagement. A bicycle presta valve, sealed with two-component Akfix epoxy, created a strong, leak-proof connection between the compressor and housing. Housing cap assembly integrity was ensured using M5 nuts and bolts, and shaft balancing was ensured by attaching interchangeable M10 nuts to an application-specific 3D-printed disk with built-in M10 threads. Rotor speeds were measured using a slotted optical tachometer sensor module interfaced to an Arduino Uno R3, which was programmed using the Arduino IDE to record real-time RPM values. The Arduino RPM measuring code is shown in Appendix B.

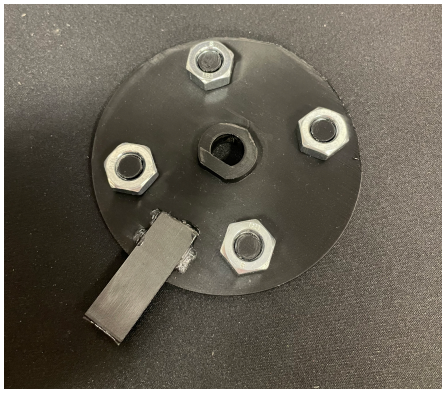

Figure 9. Disk with weights for testing

Figure 10. Presta valve

3.5. Simulation Setup

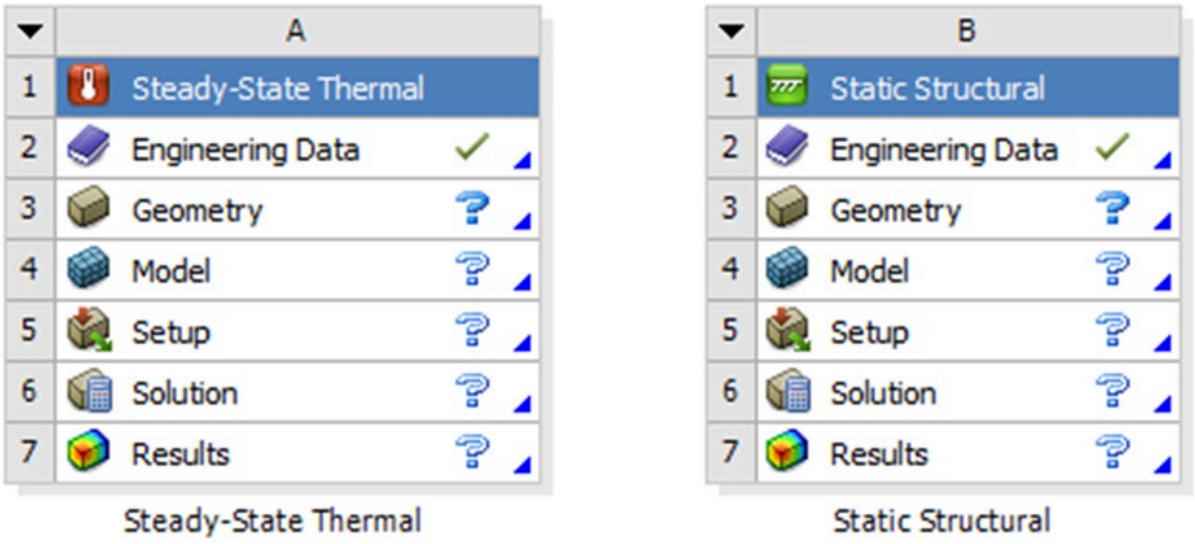

Figure 11. Systems used in the ANSYS simulation.

For the simulation of both the Wankel and liquid piston rotary engines, a static structural analysis and steady-state thermal analysis were chosen due to the inability to create a dynamic model for the characteristically rotating rotor. Without a moving rotor, the combustion process could not have been simulated directly. Instead, static structural analysis was employed through the encapsulation of the pressure coming from the air compressor apparatus in the laboratory, maintained at 8 atm. Pressure was applied to the face of the rotor opposite to the inlet from the air compressor tubing. This method succeeded in simulating pressure forces acting over the rotor's surface during engine operation. This simulation was carried out with a material that does not exactly match the actual material in the experiment due to the unavailability of the exact material in the ANSYS material library. The best possible choice for a material for the simulation was made to be as close to the material present in the experimental setup as possible.

For thermal analysis, boundary conditions were established to mimic the high temperatures encountered during combustion. One of the rotor faces, that on which combustion takes place, was set to 2500 K based on a temperature value retrieved from Spreitzer J. et al. [3], where the same rotary engine was simulated. This temperature is the highest temperature of the combustion zone. On the basis of this temperature, the heat flux determined the combustion face. Conclusively, in the thermal simulation, the rotor housing temperature was

kept at a reference temperature of 250K for purposes of simulating effects of environment cooling because it is that ambient temperature in most of such simulations.

These boundary conditions helped the simulation to estimate the thermal behavior, as well as heat transfer characteristics of the engine components under operating conditions in which the effect of dynamic rotor movements was not considered in the analysis. This given setup would then be such that it provides insight into thermal stresses and heat fluxes that the engine components would normally experience during normal operation but would not actually be able to simulate the full dynamic combustion process.

Simulation Parameters for Internal Combustion:

- **Wankel Engine:**
  - **Compression Ratio:** ~10:1
  - **Operating Condition:** Typical automotive RPM range of 3000-6000 RPM. Stoichiometric air-fuel ratio for gasoline combustion.
- **LiquidPiston Engine:**
  - **Compression Ratio:** 9:1 [16]
  - **Operating Condition:** Typical automotive RPM range of 3000-6000 RPM. Stoichiometric air-fuel ratio for gasoline combustion.

Boundary Conditions:

- **Intake:**
  - Uniform air-fuel mixture at ambient conditions, which are 25°C, 101.3 kPa.
  - Controlled mass flow rate to reflect real world intake dynamics.
- **Combustion Chamber:**
  - Heat transfer coefficients considered to simulate thermal losses.
  - Combustion modeled with standard flame propagation rates for gasoline.
- **Exhaust:**
  - Pressure based outlet to simulate back pressure effects on engine performance

Validation:

Simulation results afterwards will be compared to available data from existing literature. Firstly will be checked if they align with written data. For instance, thermal efficiency will be compared to 20%-30% for Wankel and 45% for LiquidPiston [5].

4. Results

4.1. Simulation

4.1.1. Static Structural Simulation.

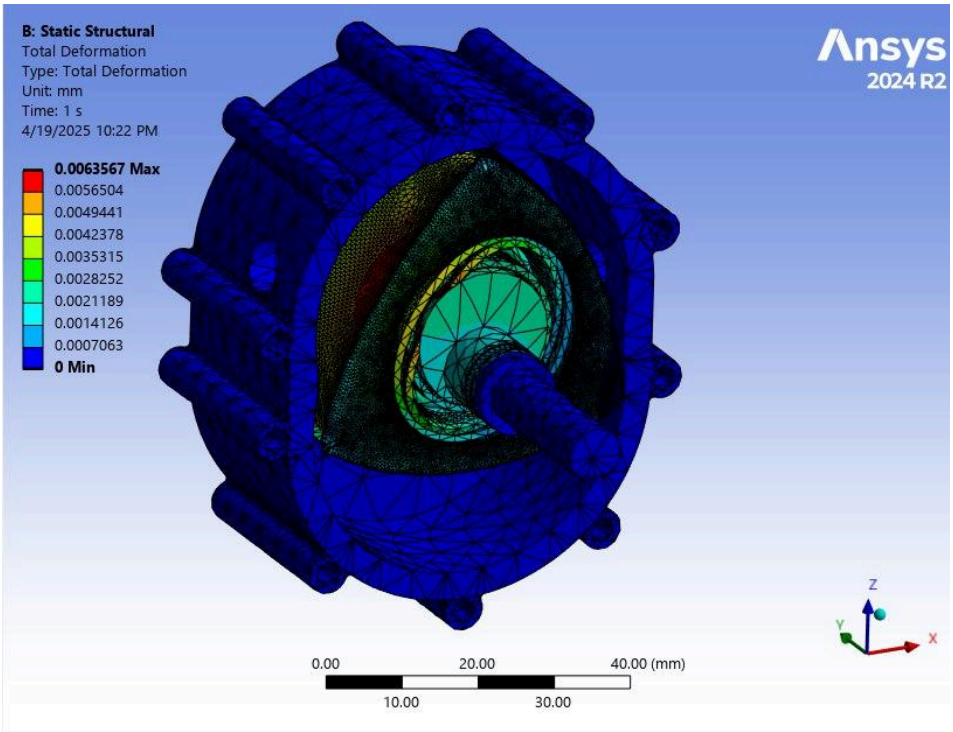

Figure 12. Static structural analysis, Total Deformation of the Wankel engine under 8 atm pressure.

Liquid Piston Engine:

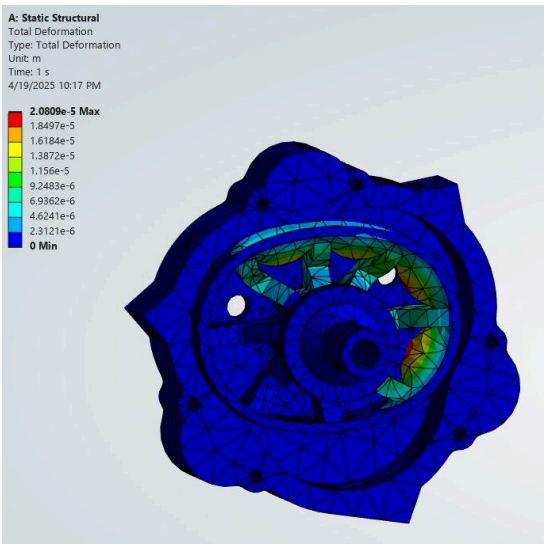

Figure 13. Total Deformation

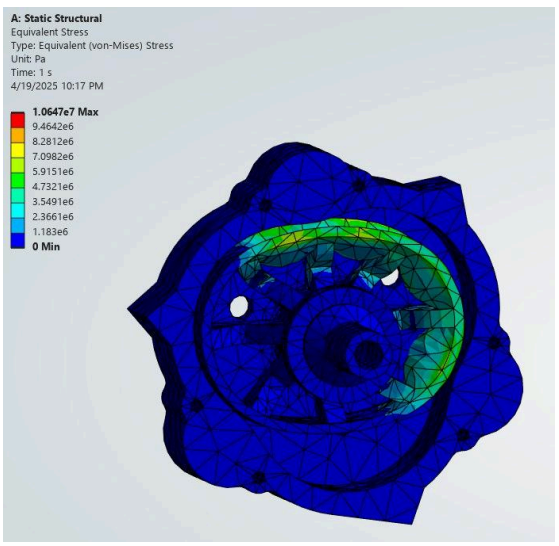

Figure 14. Equivalent (von-Mises) Stress

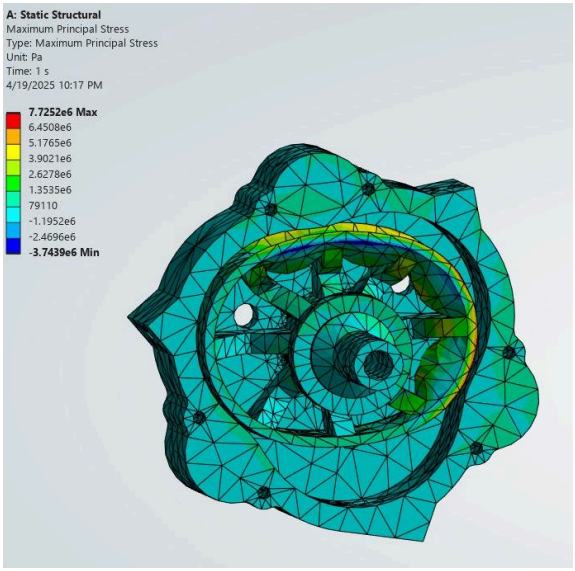

Figure 15. Maximum Principal stress

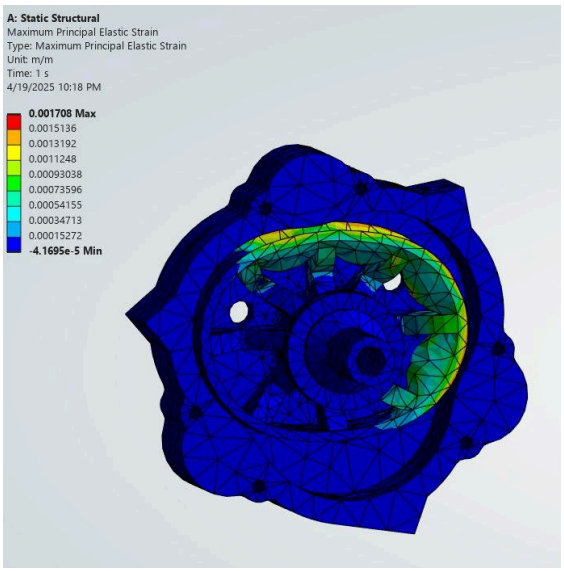

Figure 16. Maximum Principal Static Strain

In order to evaluate the structural integrity of our rotary engines, simulations were carried out using ANSYS software, which is available through the computer laboratories of our university using student access. Durability tests at high pressure were applied to the Wankel and LiquidPiston engine models, with the focus on their structural integrity.

The simulation scenario included subjecting the inlet to an internal pressure of 8 atm, which would represent normal operating conditions when hooked to an air compressor. The aim was to assess how the structures of the engines would fare under this heavy load.

The results show that the engine types undergo distinct deformation effects when rigidly constrained at the shafts. ANSYS-derived figures reveal areas of concentration of stress and displacement of the materials. This is more evident around the rotor housing and shaft connections. This indicates that the materials or even the design geometry may not be strong enough to keep its integrity at 8 atm because of deformation, given the established fixed boundary conditions.

These findings seem to imply that the shaft supporting structures should be re-evaluated, and some adjustments made to the material properties or even thickness of the engine walls should be done to ensure stability in structural performance as well. These will serve as reference results for the future-in-design, where the structures will include more reinforcements or alternative methods of restriction.

4.1.2. Simulation of Heat Distribution in the Rotary Wankel Engine

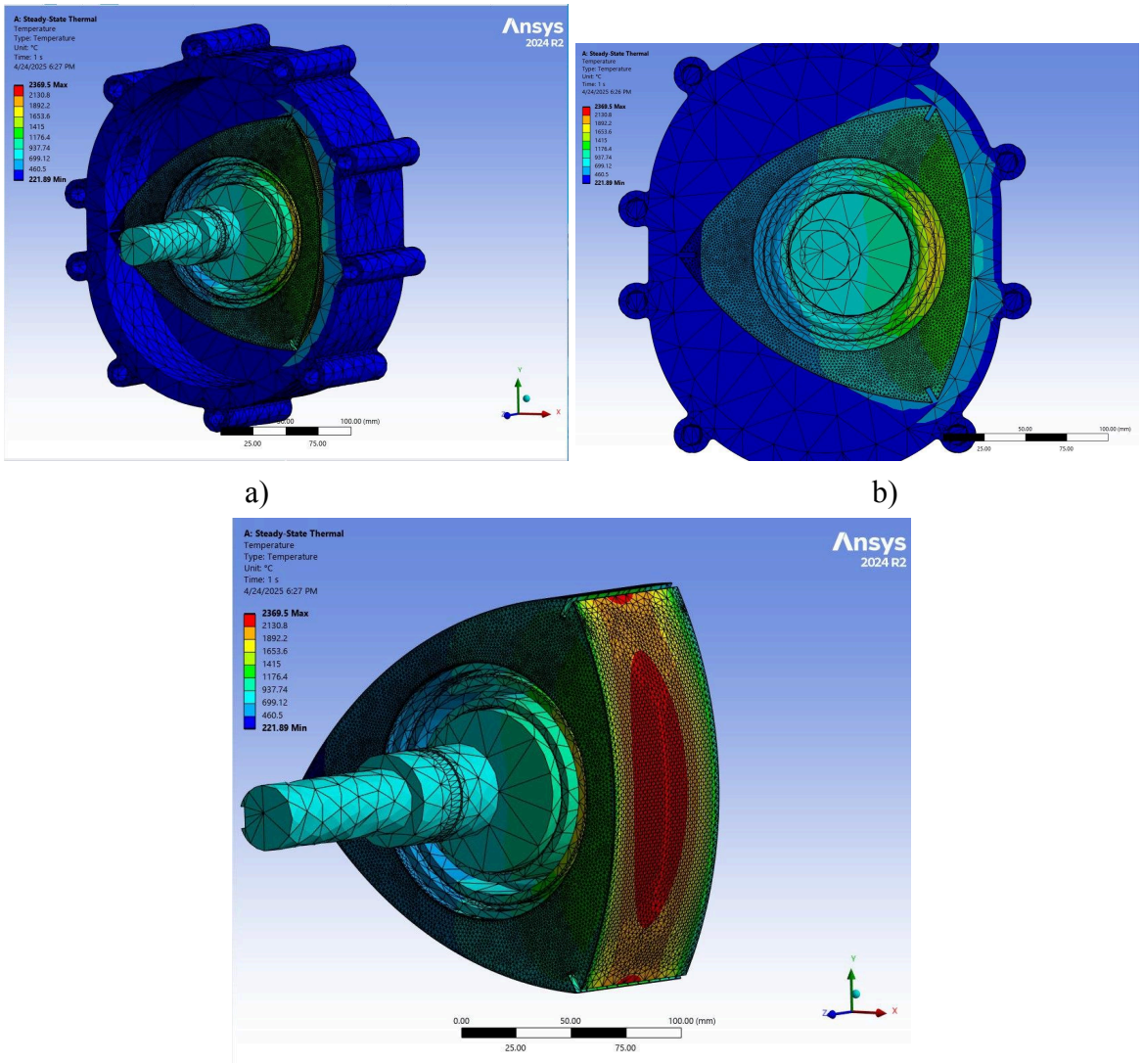

a) b)

c)

Figure 17. a) Isometric and b) front views of thermal analysis of the Wankel rotary engine, c) isometric view of the thermal analysis of the rotor.

As depicted in the above figures, the simulation was carried out for the study of the heat distribution within the rotary Wankel engine under the hypothesis that the maximum temperature for the rotor face, where combustion occurs, reaches 2500 K.

$$q = -k\Delta T/\Delta x \quad (3)$$

This is an applicable peak heat flux derived using the Stefan-Boltzmann law (3) which was calculated to be about $2.21*10^6$ W/m^2. The picture shows the simulation developed by the engine rotor surface temperature profile, which manifests the thermal range along with its extended areas. The results show dispersion of temperature to yield increase at environment temperature, with the greatest amongst them reaching up to 2369.5 K around the combustion chamber area. Heat flux leads to a considerable temperature gradient, pointing to possibly higher thermal stress areas that need further consideration in a material perspective. These results correlate well with the engine's expected behavior at elevated operating temperatures while forwarding the thermal management and optimization for engine design.

4.1.3. Simulation of Heat Distribution in the LiquidPiston engine

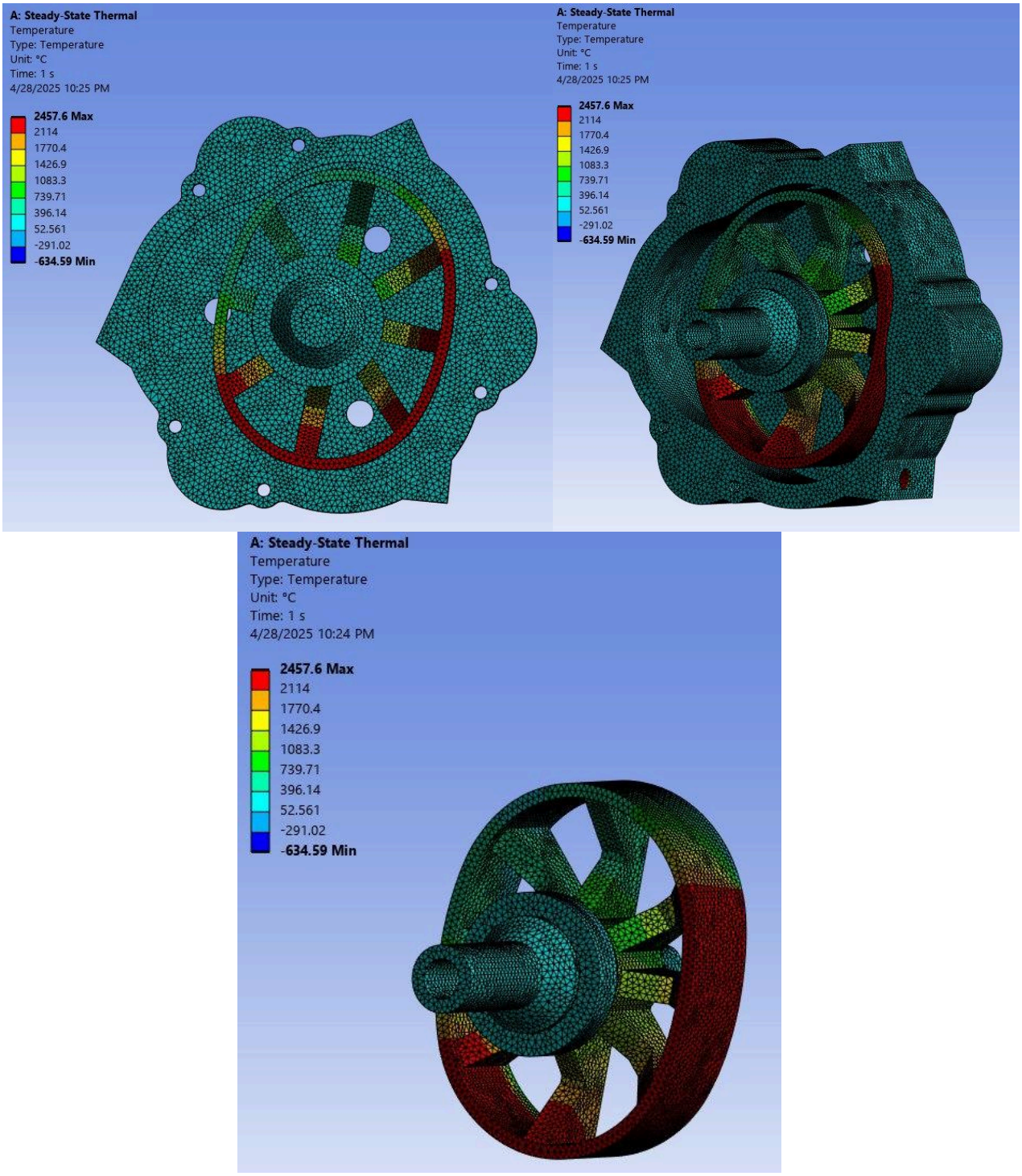

Figure 18. a) Isometric and b) front views of thermal analysis of the Wankel rotary engine, c) isometric view of the thermal analysis of the rotor.

The simulation of the LiquidPiston's operation at the combustion chamber is done to

analyze thermal distribution across the engine. The simulation's assumption is that the rotor face's maximum temperature equals ~2500 K, same as the Wankel Engine. By using the max temperature the heat flux can be evaluated by the Equation (1). Input heat flux is determined to equal $2.21*10^6$ W/m^2. Figure 15 provides detailed results of temperature distribution across the LiquidPiston engine. The highest temperature (2500^o C)is located at the rotor's face where combustion is occurring. Provided results indicate which areas should be considered first concerning materials thermal properties. Overall, the simulation results meet the experimental results provided by the [15]:

Test case	1	2
Housing temperature (K)	470	477
Apex seal temperature (K)	518	500
Front plate temperature (K)	480	483
Back plate temperature (K)	460	468

Figure 19. Steady state temperatures [15]

4.1.4. Comparison Between LiquidPiston Engine and Rotary Wankel Engine Simulation Results

In both simulations, similar conditions of the combustion chamber are used to describe their structural and thermal properties. Both engines experienced the same 8 bar pressure which is simulating the compressed air circumstances that the report's experimental part is approaching. For the thermal analysis, the combustion temperature of 2500 K is set to compare their thermal distribution results. Wankel Engine's structural simulation demonstrated higher deformation especially near the shaft area and rotor. The near shaft area and housing materials can be changed to a stronger material to improve performance. The LiquidPiston engine also experienced deformation under 8 bar pressure. However, the stress distribution is uniformly distributed compared to the Wankel engine's stress results. Comparing both engines LiquidPiston demonstrated better results on material's ability to withstand high pressure conditions, while Wankel Engine showed higher deformations on

the same 8 atm pressure condition. The LiquidPiston engine showed decreased mechanical failure risk and better durability compared to the Wankel Engine.

In the Wankel engine's results very high concentration of the heat/high temperature is observed at the combustion chamber. According to the graph, the temperature gradients are sharp and these spots should attain the main attention in terms of materials potential high temperature failures. In the both simulations the setup condition is peak combustion temperature 2500 K and heat flux condition is calculated to be equal $2.21*10^6$ W/m^2. These assumptions are done according to the [3] source's provided data. On the contrary to the Wankel engine, the LiquidPiston engine showed a more uniform distribution of the temperature. Overall, the LiquidPiston's thermal distribution shows that its geometry, shape is more efficient compared to the Wankel engine's configuration. Moreover, it says that Wankel engine's rotor material requires more thermal performance and is more likely to experience thermal failure compared to the LiquidPiston which has higher durability.

4.2. Build and Issues

The experimental prototypes were printed on a Bambu Lab X1E with PETG filament, 25% gyroidal infill, six walls, and 0.2 mm layer height. The print bed temperature was set at 80 °C to minimize warping, and the orientation was such that overhangs were the smallest possible. No supports were placed on key sealing surfaces to avoid compromising dimensional integrity, and components were left to cool prior to removal. Mid-print, the work stopped to insert M5 nuts into the housing walls to be fastened later with caps. The prints then continued to completely encase these inserts. A Presto valve cartridge was inserted into its special port and secured with Akfix two-component epoxy, and the intake was equipped with a bicycle spoke nipple adapter to connect to the compressor. Housing caps were fastened with M5 bolts.

Shown in Figure 18, early assembly without housing caps ensured precise reproduction of the cycloidal and trochoid geometries. Bearing pockets were inspected with calipers by hand and then populated with deep-groove ball bearings, 6004Z on the rotor and 6001Z within the housing, which seated smoothly without damage. Apex seals were installed and coated with graphite powder lubricant for low-friction contact.

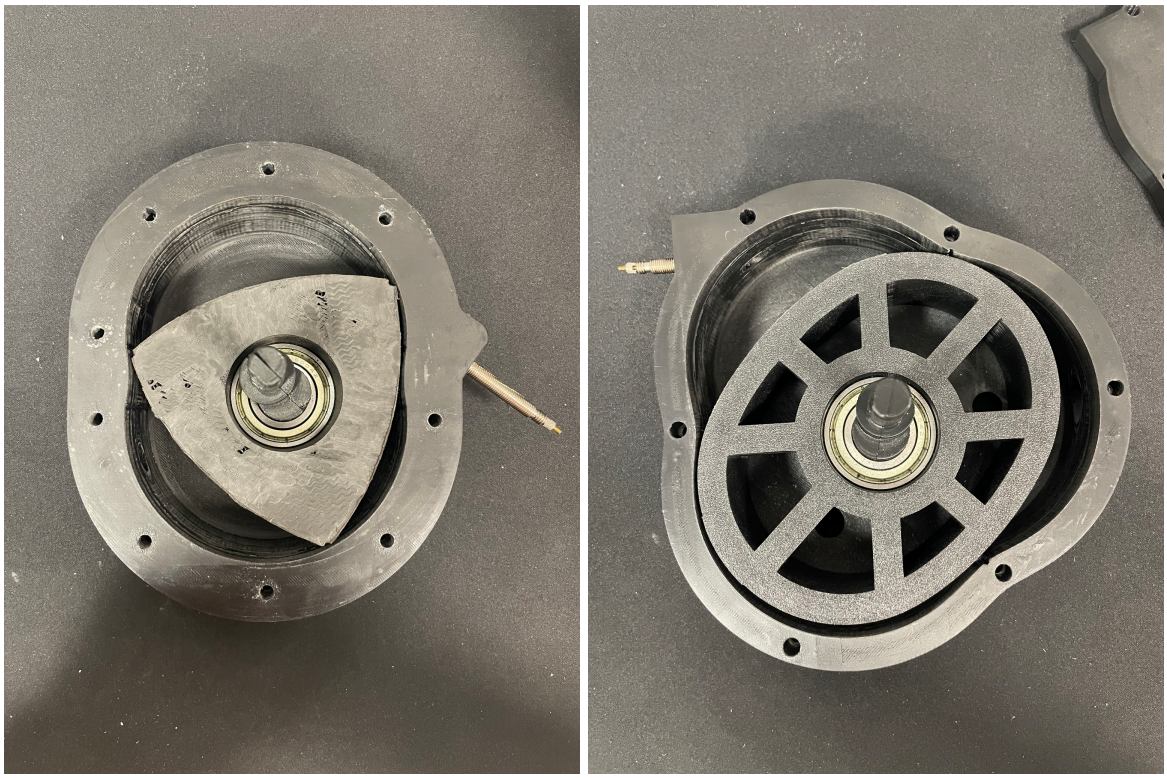

Figure 20. 3D printed Wankel and LiquidPiston engines with open housing

Upon tightening the caps on the housing (Figure 19), rotational resistance grew significantly. With caps off, rotors turned freely by hand and had good geometry and lubrication. Upon the caps being tightened, rotational resistance significantly grew compared to the un-capped condition, reflecting increased binding upon load. The sanding of the rotor edges to generate clearance did not decrease the resistance, which implies that the rotor tips were rubbing against the chamber walls because of minute shaft misalignment within the housing bore.

Fully assembled prototype units were attached to the compressor for constant 5 atm testing (Figure 20). On the first test, the pressure was gradually ramped but the compressor was not able to overcome the assembly friction and there was no motion of the rotor. On the second trial, full pressure was applied suddenly and that too did not initiate rotor motion. Moreover, the interference fit of the bearings can cause non-uniform preload due to the differences in pocket tolerance, which can actually lock the rotor under load. The inherent anisotropic layer features and residual surface finish from FDM printing may also get engaged on the rotor edges, enhancing the static friction. All these findings imply that assembly tolerances, specifically the shaft alignment and precision of bearing seating, need to be improved upon, and then only the compressor-based testing can successfully proceed.

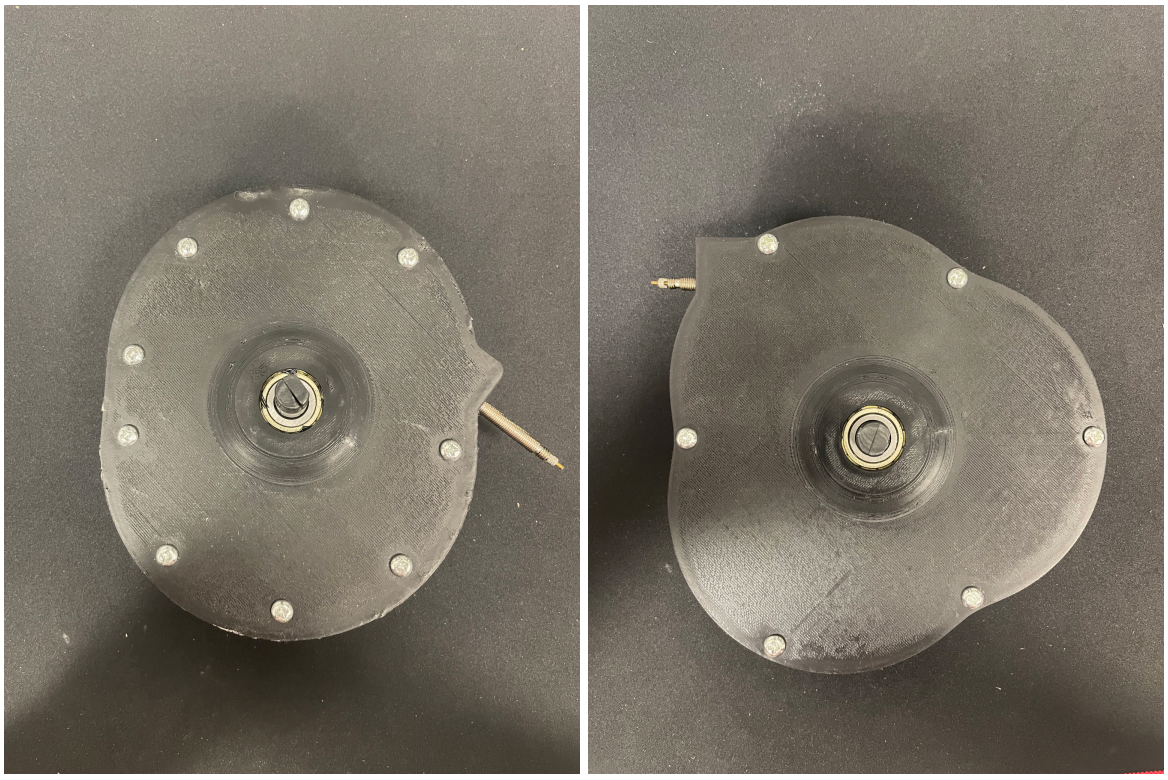

Figure 21. 3D printed Wankel and LiquidPiston engines with closed housing

Figure 22. 3D printed Wankel and LiquidPiston engines connected to compressor

4.3. Future Recommendations

There are several future suggestions for this project. Firstly, expanding existing static analyses to fully coupled, time-dependent simulations will provide higher predictive accuracy and deliver the actual dynamic response of the engines. Moving-boundary CFD and FEA models that include simulated rotor motion, seal-tip interaction, and cyclical heat transfer will provide unsteady pressure waves and transient thermal loads during each engine cycle and guide design optimizations prior to prototype manufacture.

Secondly, to enhance the performance of the 3D-printed prototypes, there are various improvements to the testing procedure to be instituted. The use of precision shaft alignment fixtures or bushings will avoid binding through the elimination of bearing runout. Quantitative leak-down tests on printed housings can then determine per-cycle air loss, and surface treatments of thin-film polymer liners or integrated O-ring grooves can then be implemented to minimize leakage and enhance compression retention. Improved lubrication techniques should be explored and compared to graphite powder to determine the best lubricant for the cyclic engine operation. The optimization of seal geometries should also consider the balance between sealing performance and rotational friction. Stereolithography printing should also be looked into as an alternative to FDM to achieve greater dimensional accuracy and improved structural integrity in critical engine components. The use of a compressor with greater flow and pressure capacity or reprinting the prototypes at a smaller scale would increase the ratio of pressure to area, and the potential to overcome static friction in subsequent testing.

Lastly, production of both the LiquidPiston and Wankel engines using the desired metal materials (for example, aluminum 6061-T6 or an appropriate steel alloy) will prove the concepts in actual operating conditions. The prototypes in metal will reflect true thermal conductivity, structural stiffness, and wear, and actual thermal efficiency, top rate of RPM, and power-to-weight ratio can be measured directly. Measuring these values against published performance data for the XMv3 will establish the feasibility of the designs and inform further improvements.

4.4. Analysis and Discussion

The results of the project thus far have provided valuable information into the design of both engines, and their performance metrics were collected from literature review for further comparison with simulation and physical test results. So far primary focus has been on design and 3D modeling and preparations for next steps. But all that work sets the foundation for future works to be done.

Considering the large amount of literature about Wankel engines, the 3D model design and modeling process was straightforward. And further remodeling it for 3D printing and testing required knowledge obtained from previous courses and experience. On the other hand, due to lack of literature on the unreleased LiquidPiston engine, the design and 3D modeling process exceeded the amount of time initially anticipated. So far, a simple model for 3D printed tests is ready considering its simplicity.

On the theoretical part information on performances were collected from various literature available. So far comparison on the basis of this information only shows the promising potential of LiquidPiston engine over Wankels engine. Thus tests and simulations are expected to validate these expectations.

Future simulations are expected to give more information about performances in desired metrics for further comparison. For thermal efficiency, Wankel engine is expected to show thermal losses higher than LiquidPiston engine. Durability analysis will likely confirm the LiquidPistons advantage on that metric, by showing less wear and less stress on materials.

The physical tests with 3D printed models are expected to give additional information on pure physical properties considering usage of pressurized air instead of combustions. Resulted torque values will validate simulation results on that matter.

Comparatively, the LiquidPiston engine's emphasis on efficiency and emissions makes it a promising candidate to use for various applications, from transports like cars or UAV to compact portable generators.

The experiments using 3D printing offered tangible insight into manufacturing tolerance, material response, and assembly issues. While the desired motion of the rotor was not realized, the failure exposed key sensitivity to the alignment of the shaft and to FDM tolerance. The binding that occurred on the insertion of the housing caps exposed the effect of minute dimensional variations, which would be unrealistic to characterize using simulation alone.

In addition, the experiment has identified limitations of FDM printing when exposed to cyclic loads of pressure. Although the printing accurately replicated the geometrical details, the material's stiffness and surface finish generated excessive contact friction that was higher than the compressor's torque limits. These real-world results will inform material choice and tolerance calibration for future construction, and illustrate the benefit of using rapid physical prototyping to verify design hypotheses.

5. Conclusion and Future Work

5.1. Conclusion

The key focus of the capstone project was to design, simulate, and prototype two rotary engine concepts, including a Wankel-derived and LiquidPiston-type engine, for the missions of higher thermal efficiency, structural integrity, and reduced emissions. By conducting an extensive literature survey, we set performance metrics and the relevant design parameters that guided our detailed 3D modeling and static simulation streams. We were able to achieve complete parametric CAD models, conduct thermal and structural analyses, and 3D-print full-scale prototypes for compressor-based testing.

Simulation indicated the design of the LiquidPiston is thermally more efficient and less prone to loss of heat than the Wankel variant. Experiments conducted in the real-world confirmed the validity of our approach to modeling but exposed key assembly flaws: misalignment of the shaft and material limitations of FDM limited rotor motion at below 5 atm compressor pressure. While dynamic testing data were not obtained, these failures yielded critical insights into manufacturing tolerance, seal function, and materials performance that are unobtainable using simulation.

In summary, the project closes the loop between physical prototyping and theory-based modeling, illustrating the potential and the limitations involved in the design of rotary engines. The knowledge gained in tolerance control, lubrication concepts, and material selection offers an adequate starting point for further improvements in the fields of manufacturing of metal prototypes, dynamic rotating simulation, and general experimental validation in real operating conditions.

5.2. Future Work

Fully coupled, moving-boundary CFD and FEA should be used to enhance model fidelity and reflect actual dynamic performance. These models will model rotor motion, seal-tip interaction, and cyclical thermal transfer, unmasking unsteady pressure waves and transient thermal loads to inform design improvements prior to hardware construction.

Test procedures for 3D-printed prototypes need to be improved. Fixtures for precise shaft alignment will minimize runout and prevent binding. Leak-down tests on printed housings can provide per-cycle air loss measurement, and surface finish or integrated O-ring grooves can enhance compression retention. The lubrication approach must be explored and compared to graphite powder to determine the best approach to cyclic operation. Sealing performance and rotational friction needs to be balanced through optimized seal faces. Investigating stereolithography printing can provide higher dimensional accuracy and structural integrity to critical components. Increasing the flow of the compressor or reprinting smaller prototypes can raise the pressure-to-area ratio to advance the likelihood of surmounting static friction.

The last step is metal prototype fabrication in the desired materials, including aluminum 6061-T6 or appropriate steel alloys. Tight tolerances and enhanced surface finish are possible with CNC machining. Performance testing of the metal engines under actual operating conditions will quantify thermal efficiency, top RPM, and weight-to-power ratio, and provide a basis for top-level comparison to published figures. This sequence from simulation to 3D-printed testing and then to metal prototype testing is what confirms the design concepts and brings the engines closer to real-world application.

References

[1] D. Eiermann, R. Nuber, and M. Soimar, "The introduction of a new ultra-lite multipurpose Wankel engine," SAE Transactions, pp. 218–229, 1990. Available: https://doi.org/10.4271/900035.

[2] L. Finkelberg, A. Kostuchenkov, A. Zelentsov, and V. Minin, "Improvement of combustion process of spark-ignited aviation Wankel engine," Energies, vol. 12, no. 12, p. 2292, 2019. [Online]. Available: https://doi.org/10.3390/en12122292.

[3] J. Spreitzer, F. Zahradnik, and B. Geringer, "Implementation of a rotary engine (Wankel engine) in a CFD simulation tool with special emphasis on combustion and flow phenomena," SAE Technical Paper, 2015. Available: https://doi.org/10.4271/2015-01-0382.

[4] H. Meng, C. Ji, S. Wang, and J. Yang, "A review: Centurial progress and development of Wankel rotary engine," Fuel, vol. 335, p. 127043, 2023. Available: https://doi.org/10.1016/j.fuel.2022.127043.

[5] M. Nickerson, A. Shkolnik, and K. Becker, "Preliminary development of a 30 kW heavy-fueled compression ignition rotary 'X' engine with target 45% brake thermal efficiency," SAE International Technical Papers, 2018. Available: https://www.sae.org/publications/technical-papers/content/2018-01-0885/.

[6] A. Shkolnik and K. Becker, "Stratified charge combustion techniques for enhanced fuel efficiency," SAE International Technical Papers, 2015. Available: https://www.sae.org/publications/technical-papers/content/2015-32-0719/.

[7] Z. Yang, C. Ji, X. Huang, J. Yang, and S. Wang, "Modeling and analysis of apex seal leakage in a hydrogen-fueled Wankel rotary engine," Fuel, vol. 335, p. 26734, 2023. Available: https://www.sciencedirect.com/science/article/pii/S0016236122026734.

[8] K. Yamamoto, Rotary Engine. Tokyo, Japan: Mazda Publishing, 1981. [Online]. Available: https://foxed.ca/rx7manual/manuals/REbyKenichiYamamoto-1981.pdf.

[9] LiquidPiston, Inc. (n.d.). "Development of the XMv3 High-Efficiency Cycloidal Engine.". Available: https://cdn.prod.website-files.com/5f6086e9bbbabd41a20f2984/5f61488678b009a80d75574b_Development-of-the-XMv3-High-Efficiency-Cycloidal-Engine.pdf.

[10] J. M. Herreros, M. Bogarra, A. Tsolakis, and A. P. E. York, "Study of particulate matter and gaseous emissions in gasoline direct injection engine using on-board exhaust gas fuel

reforming," Applied Energy, vol. 180, pp. 165–174, 2016. Available: https://pureportal.coventry.ac.uk/files/10789904/Herreros_AppliedEnergy_180_2016.pdf.

[11] LiquidPiston, Inc. "Frequently Asked Questions.". Available: https://www.liquidpiston.com/faq

[12] P. Fasihi, O. Kendall, P. Mutton, Q. Lai, C. Qiu, W. Yan, "Effect of graphite and MoS2 based solid lubricants for application at wheel-rail interface on the wear mechanism and surface morphology of hypereutectoid rails," *Tribology International*, vol. 157, p. 106886, May 2021, doi: https://doi.org/10.1016/j.triboint.2021.106886.

[13] C. E. Morstein, A. Klemenz, M. Dienwiebel, and M. Moseler, "Humidity-dependent lubrication of highly loaded contacts by graphite and a structural transition to turbostratic carbon," *Nature Communications*, vol. 13, no. 1, Oct. 2022, doi: https://doi.org/10.1038/s41467-022-33481-9.

[14] R. Keshavamurthy, V. Tambrallimath, A. A. Rajhi, Shabbir A. R. M., A. Y. Patil, T. M. Yunus Khan, R. Makannavar, "Influence of Solid Lubricant Addition on Friction and Wear Response of 3D Printed Polymer Composites," *Polymers*, vol. 13, no. 17, p. 2905, Aug. 2021, doi: https://doi.org/10.3390/polym13172905.

[15] Costa, T. J., Nickerson , M., Littera, D., Martins, J., Shkolnik, A., Shkolnik, N., & Brito, F. August 11, 2016. *(PDF) measurement and prediction of heat transfer losses on the XMV3 rotary engine*. Measurement and Prediction of Heat Transfer Losses on the XMv3 Rotary Engine. https://doi.org/10.4271/2016-32-0033

[16]https://cdn.prod.website-files.com/5f6086e9bbbabd41a20f2984/5f9accc0f3f8f455bebc45f3_94%20Shkolnik%2C%20Alexander_final%20paper.pdf

Appendix

Appendix A. Technical Drawings

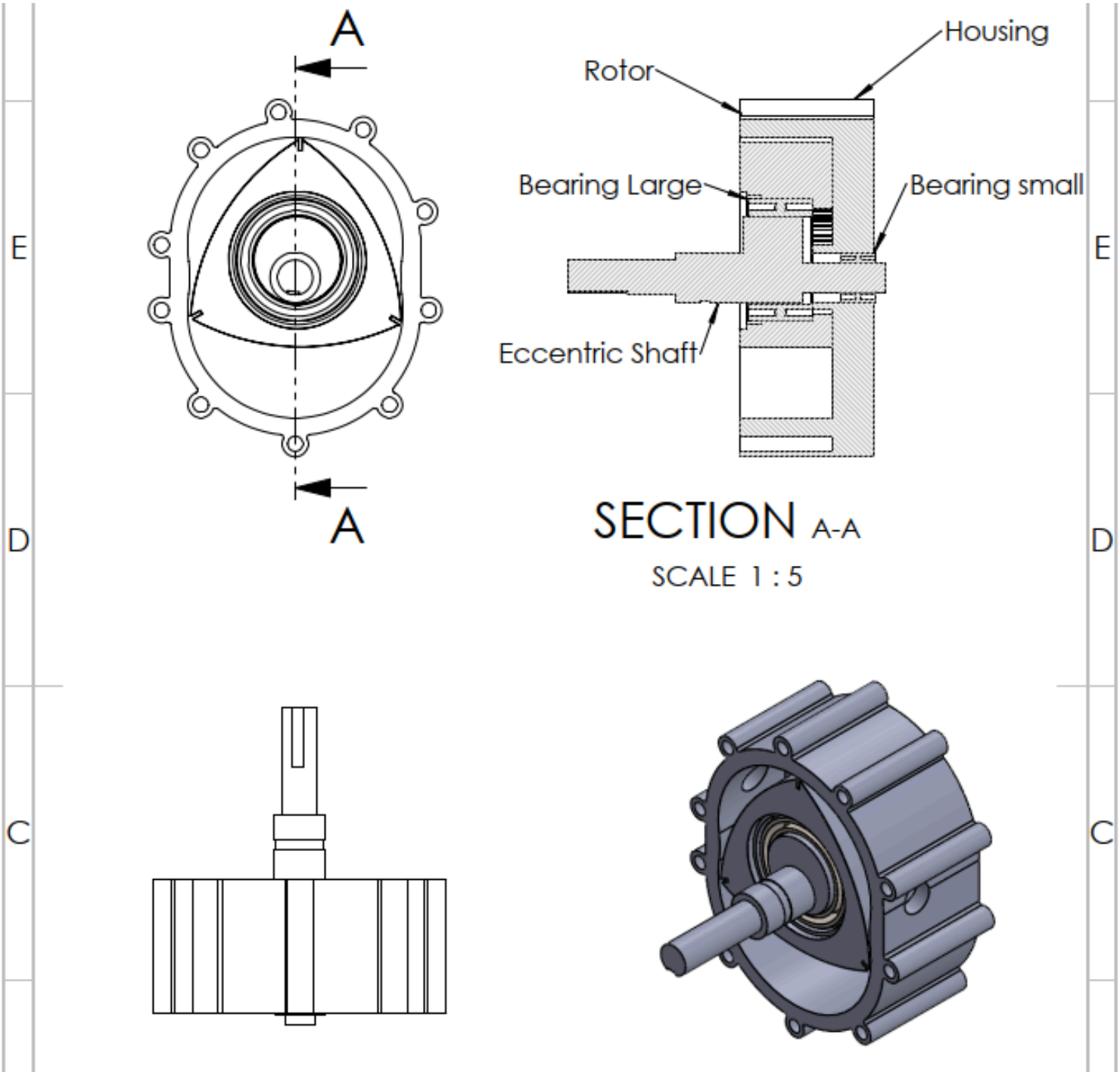

Figure 23. Wankel engine assembly for simulation with a scale 1:5 on A4 paper (without front plate to see the inside).

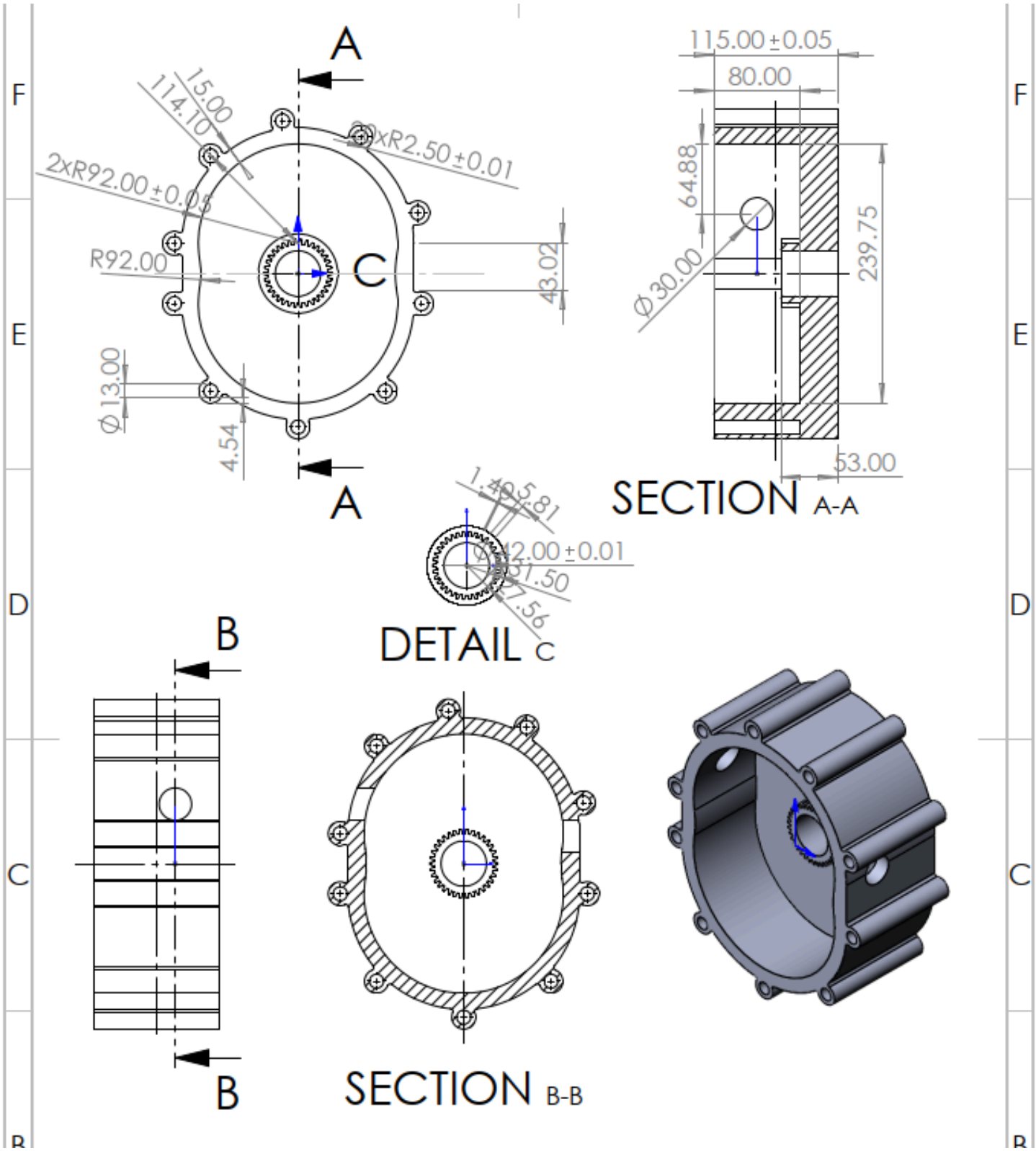

Figure 24. Wankel engine rotor housing for simulation with a scale 1:5 on A4 paper.

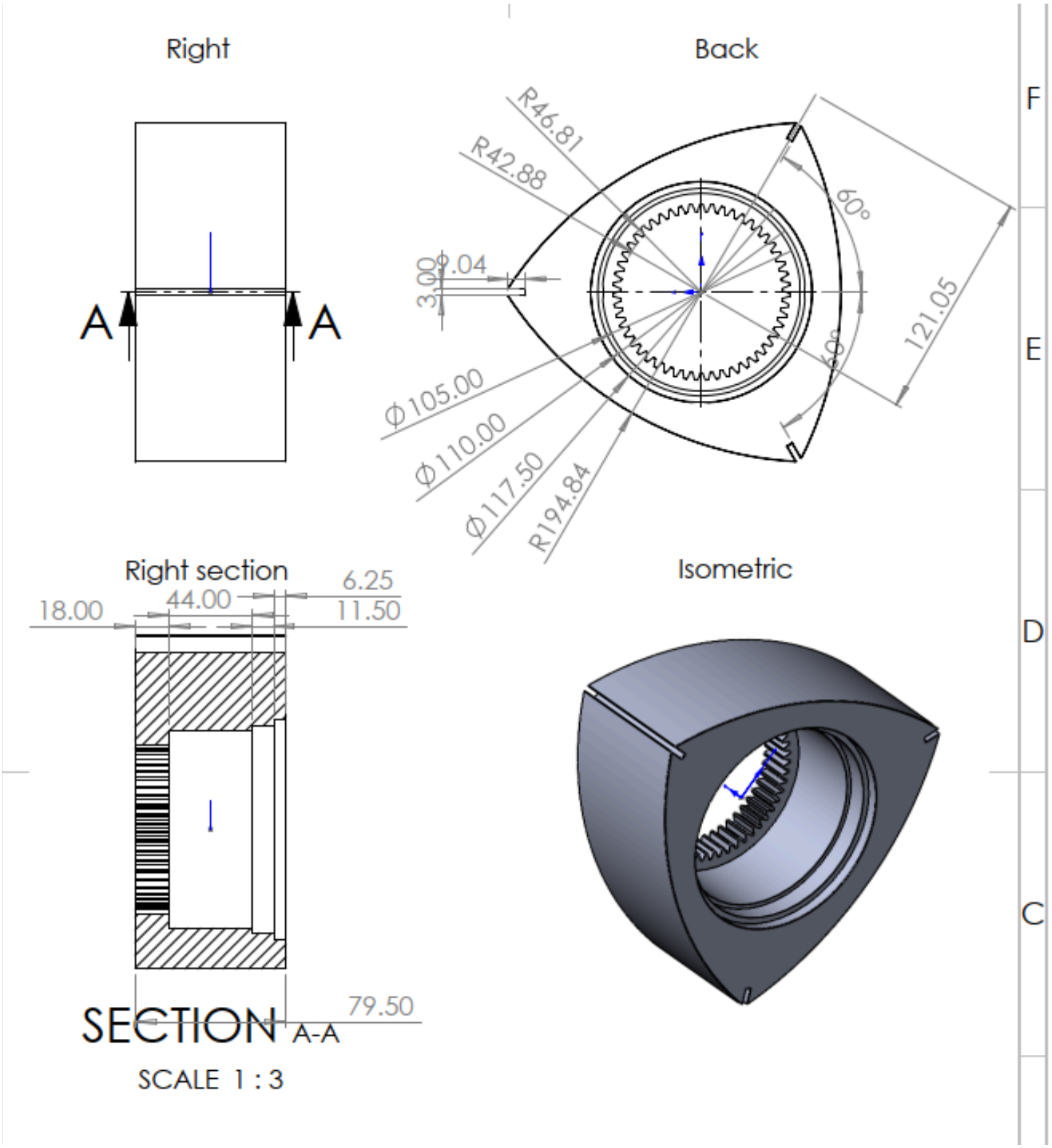

Figure 25. Wankel engine rotor drawing for simulation at a scale of 1:3 on A4 paper.

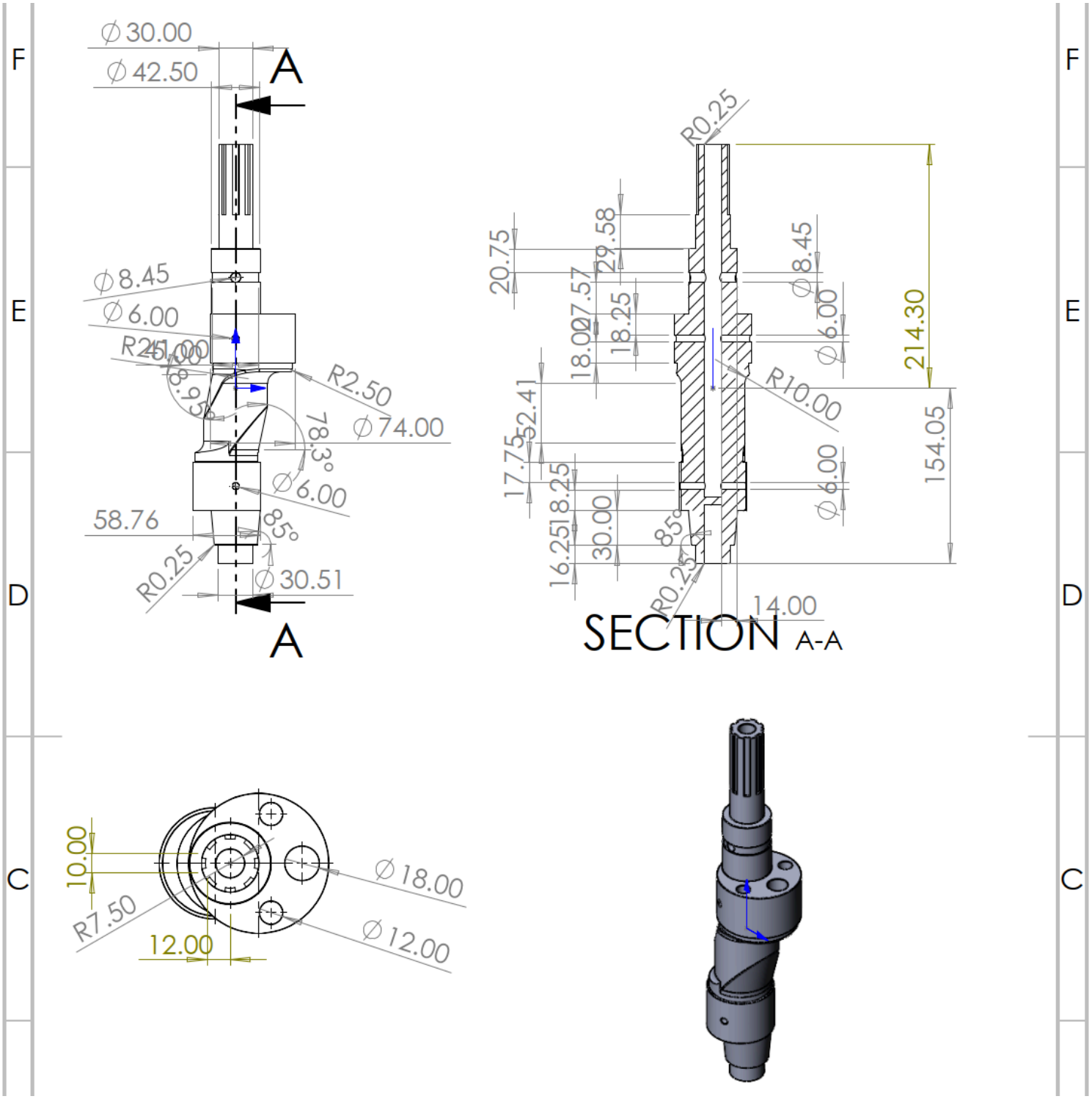

Figure 26. Wankel engine eccentric shaft drawing at a scale of 1:5 on A4 paper.

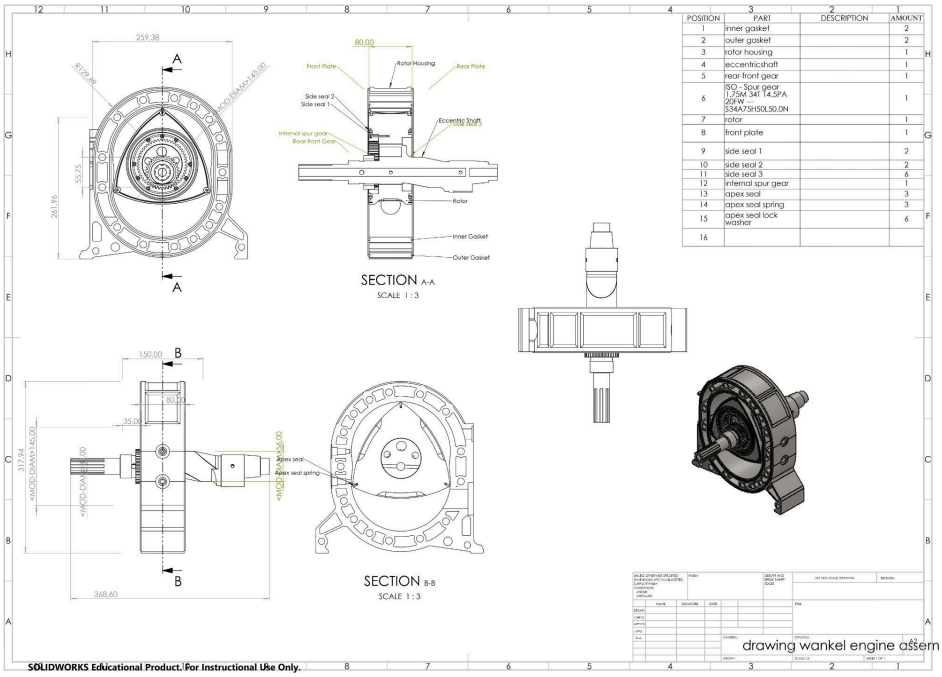

Figure 27. Wankel engine drawing

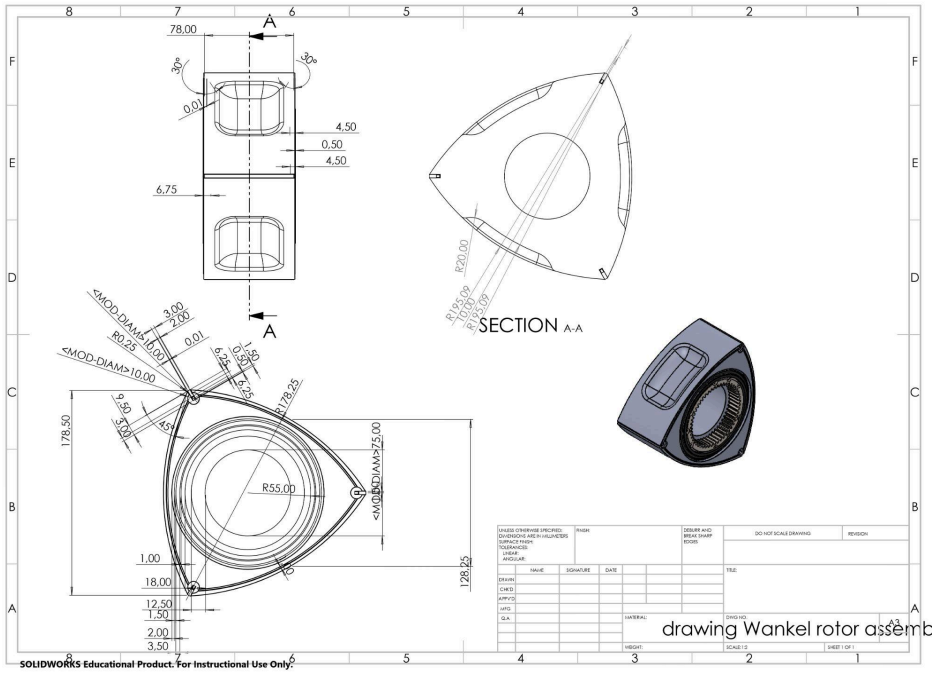

Figure 28. Wankel engine rotor drawing

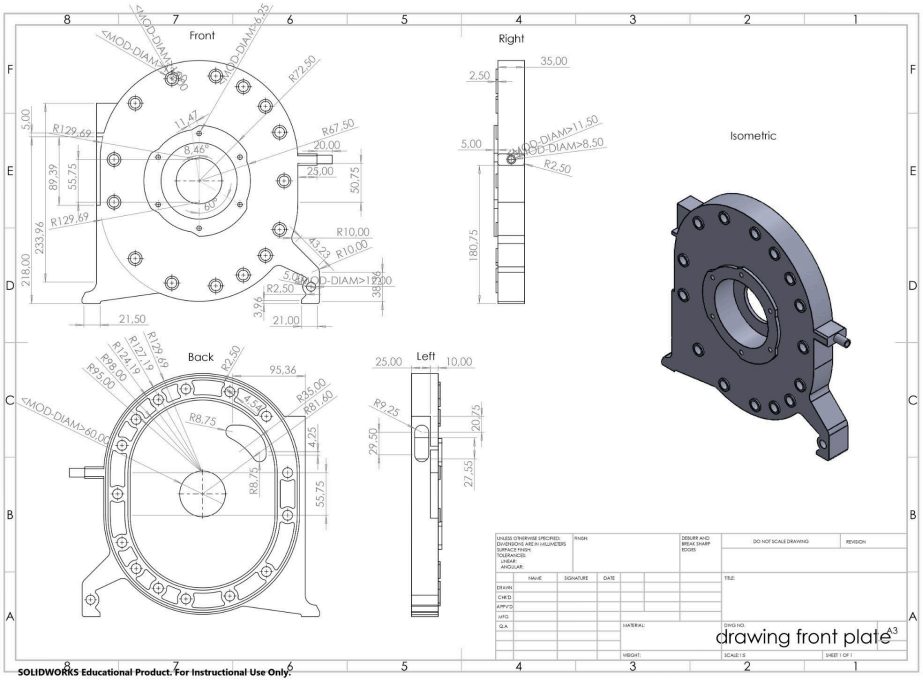

Figure 29. Wankel engine front plate drawing

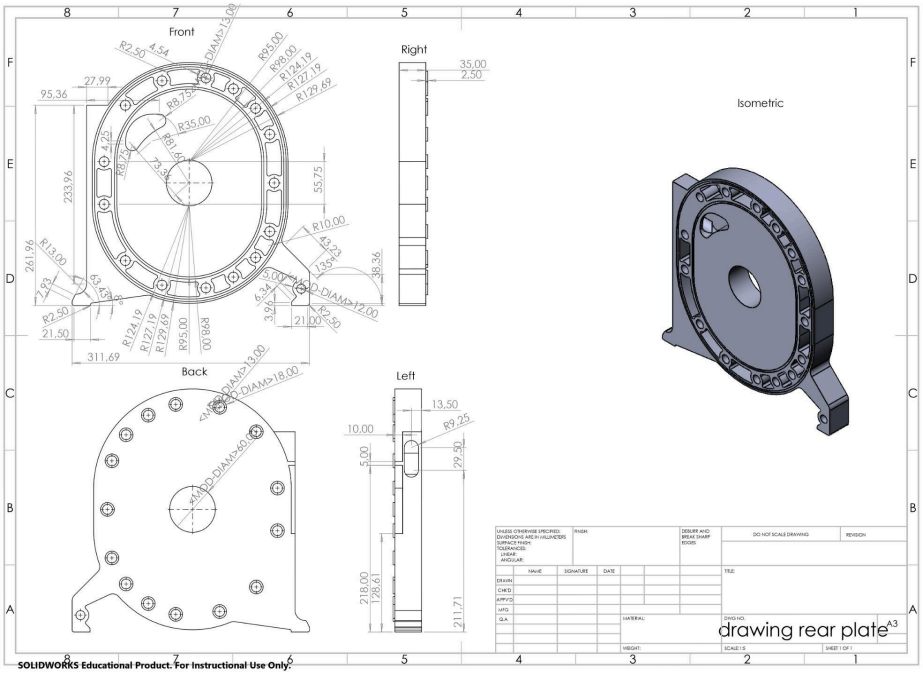

Figure 30. Wankel engine rear plate drawing

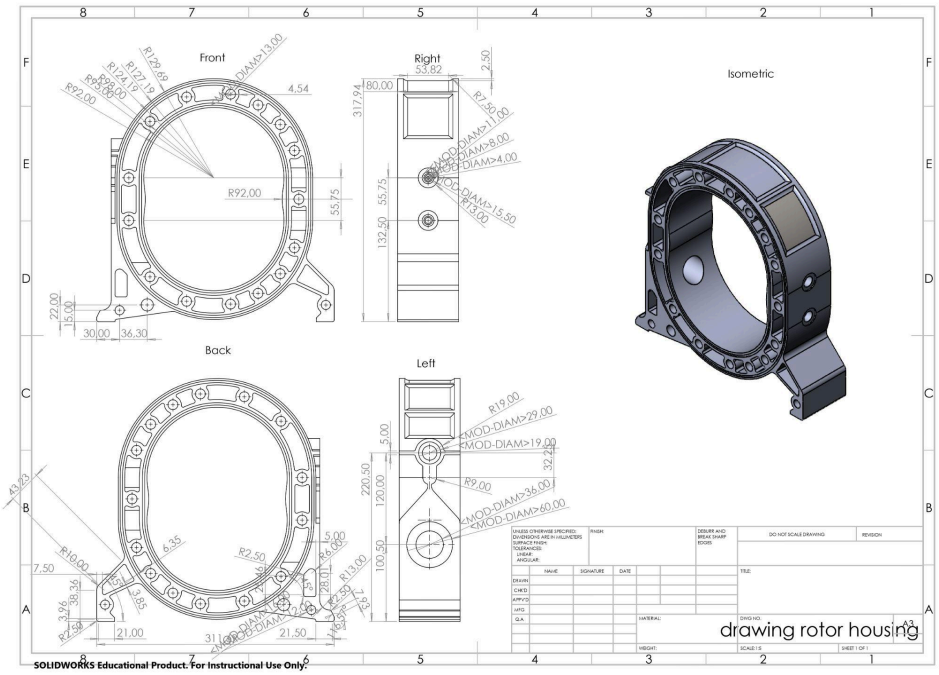

Figure 31. Wankel engine rotor housing drawing

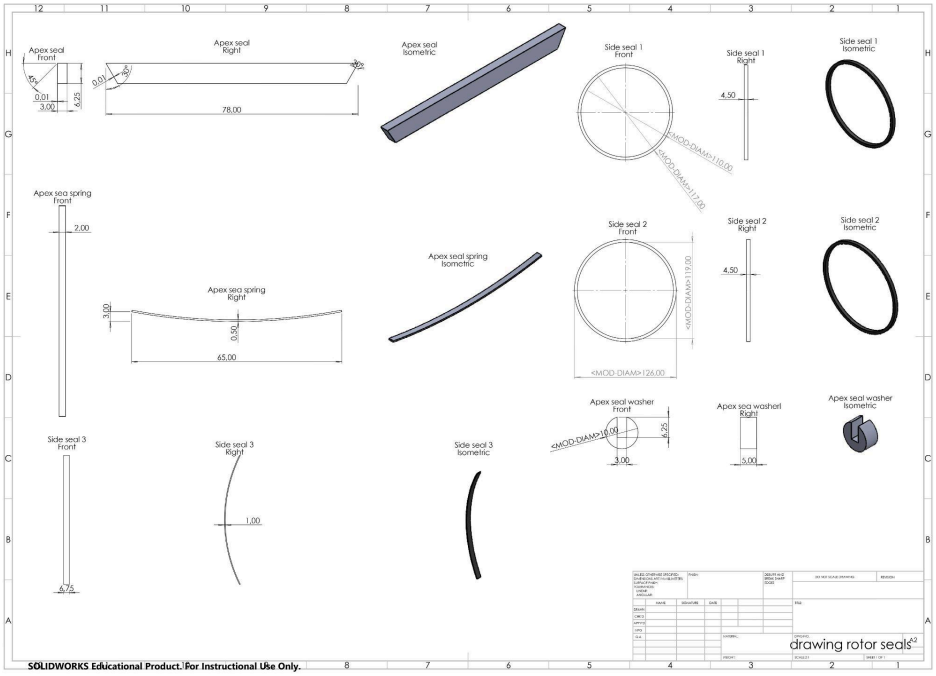

Figure 32. Wankel engine seals drawing

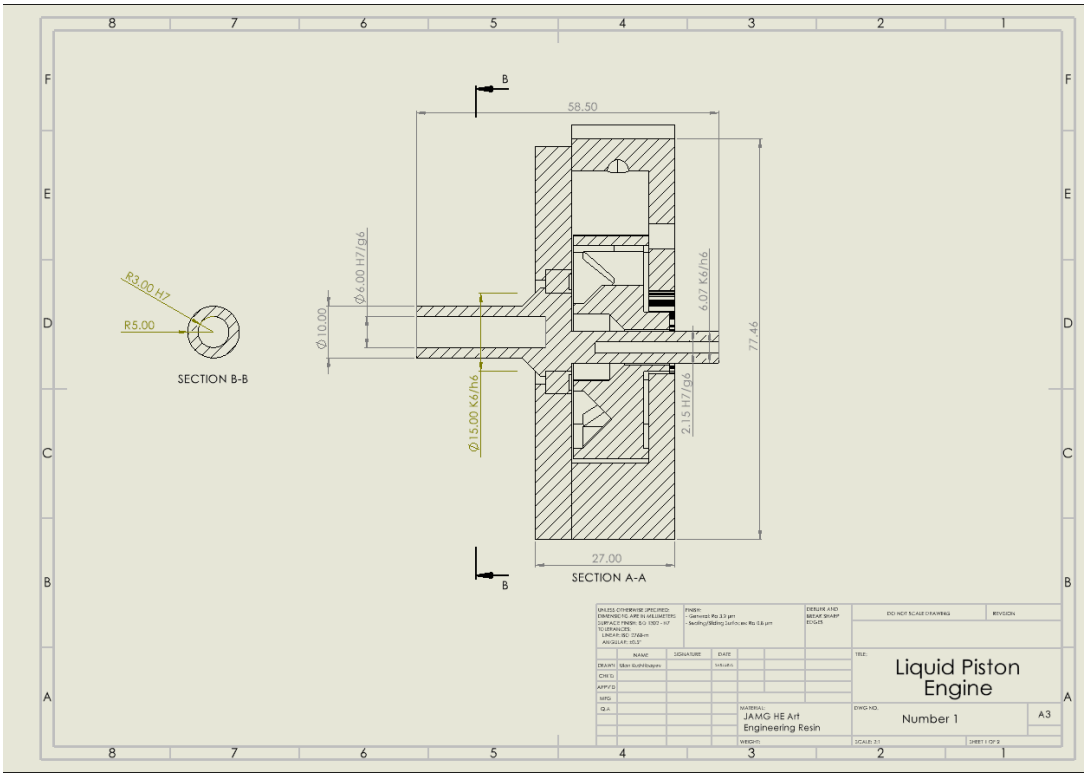

Figure 33. LiquidPiston engine section view drawing

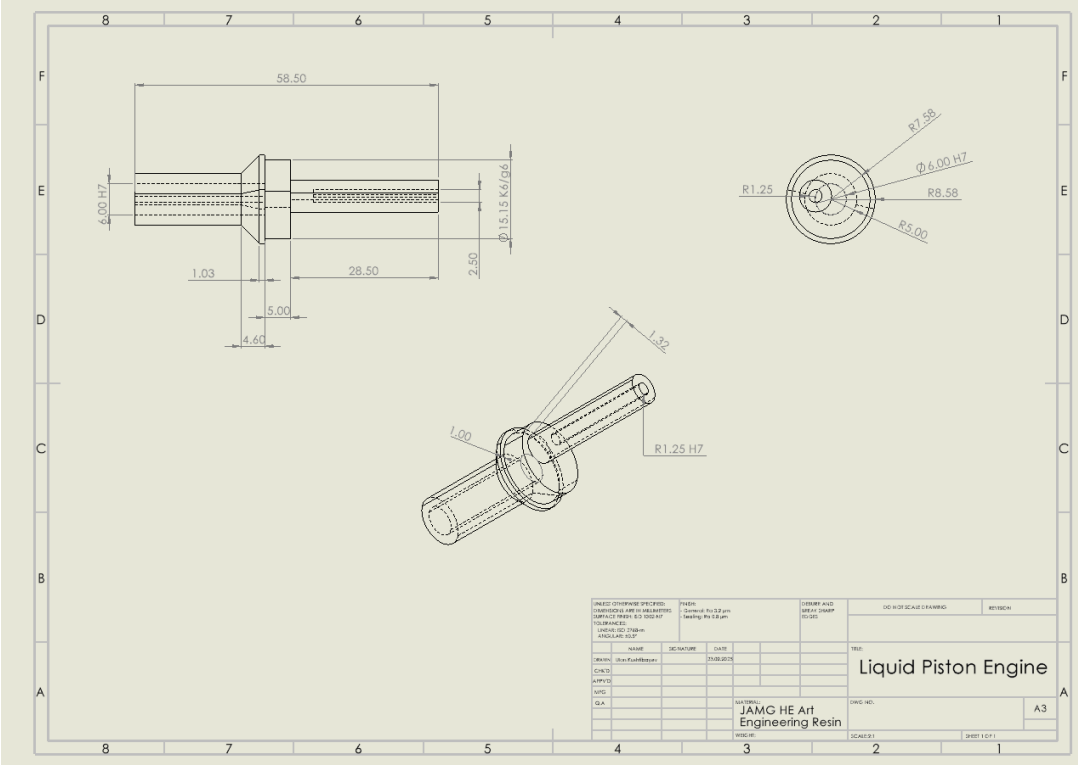

Figure 34. LiquidPiston shaft drawing

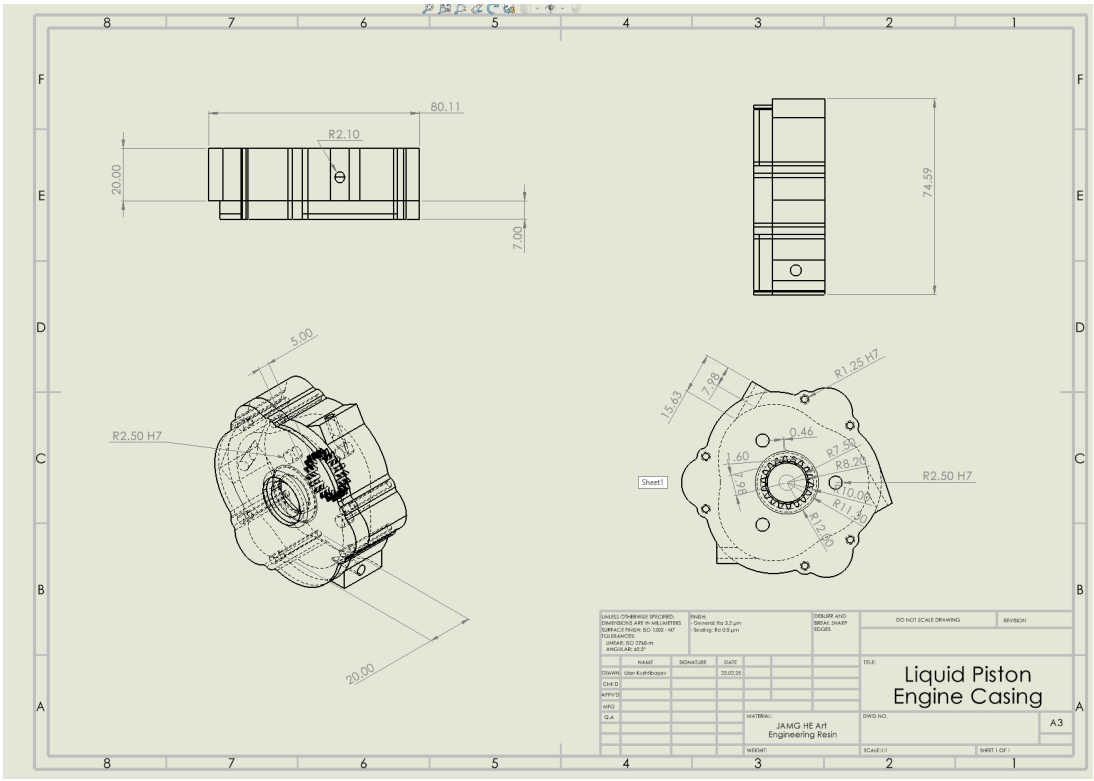

Figure 35. LiquidPiston casing drawing

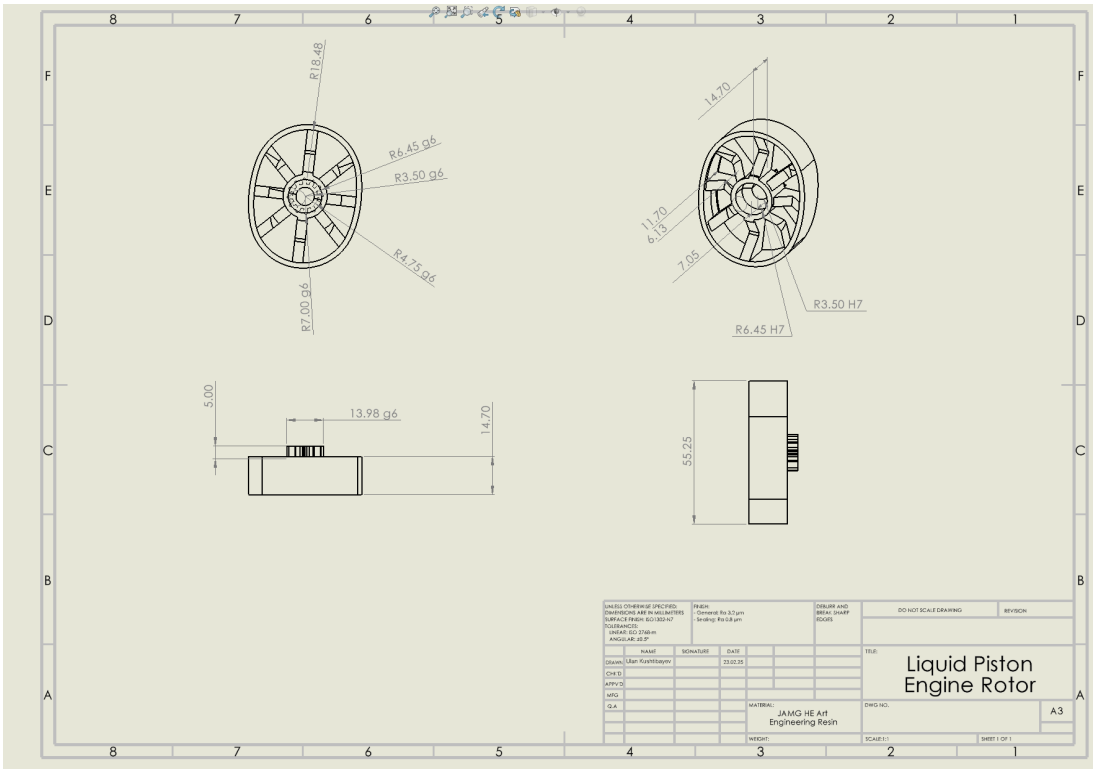

Figure 36. LiquidPiston rotor drawing

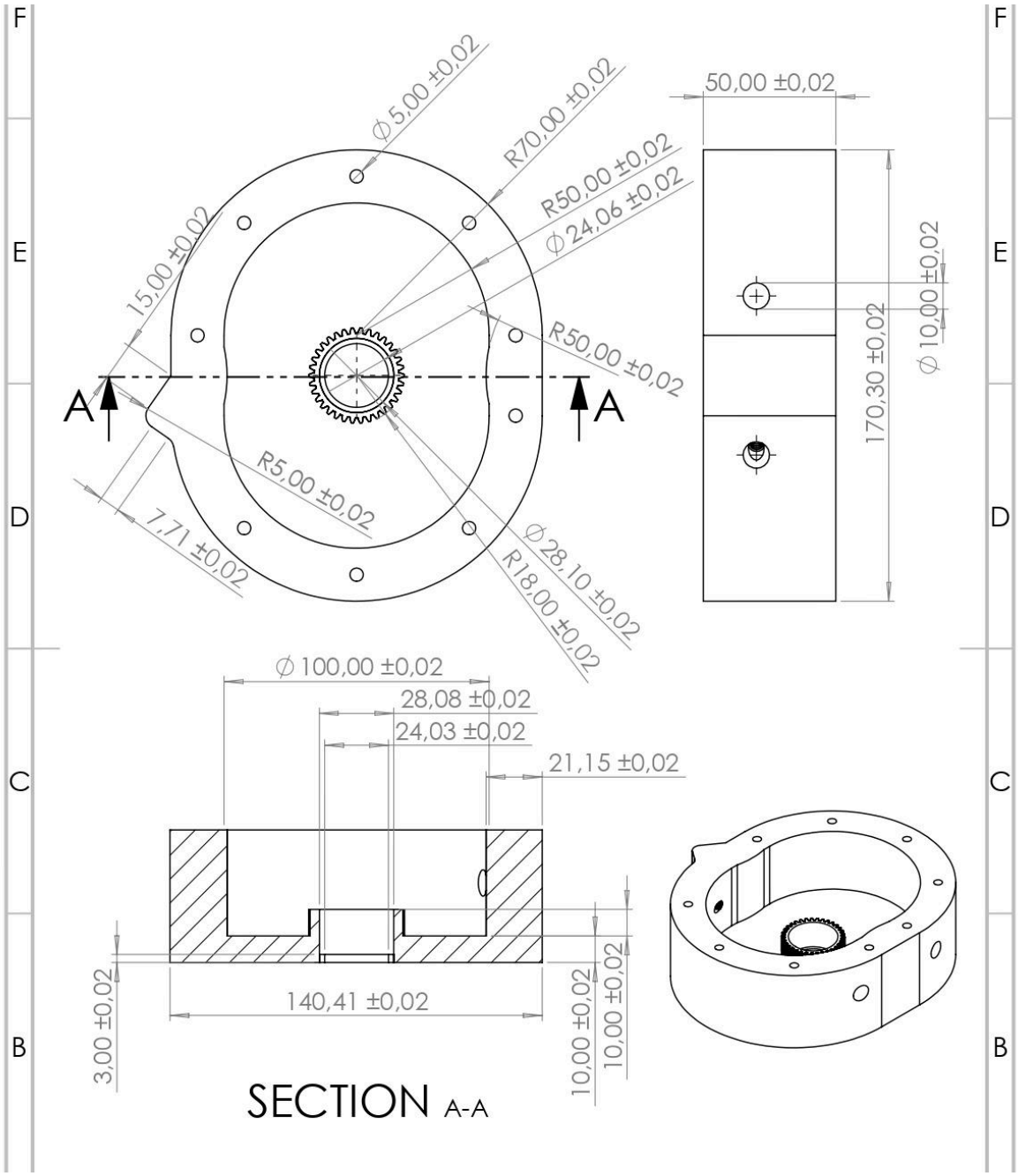

Figure 37. 3D printed Wankel Engine housing drawing

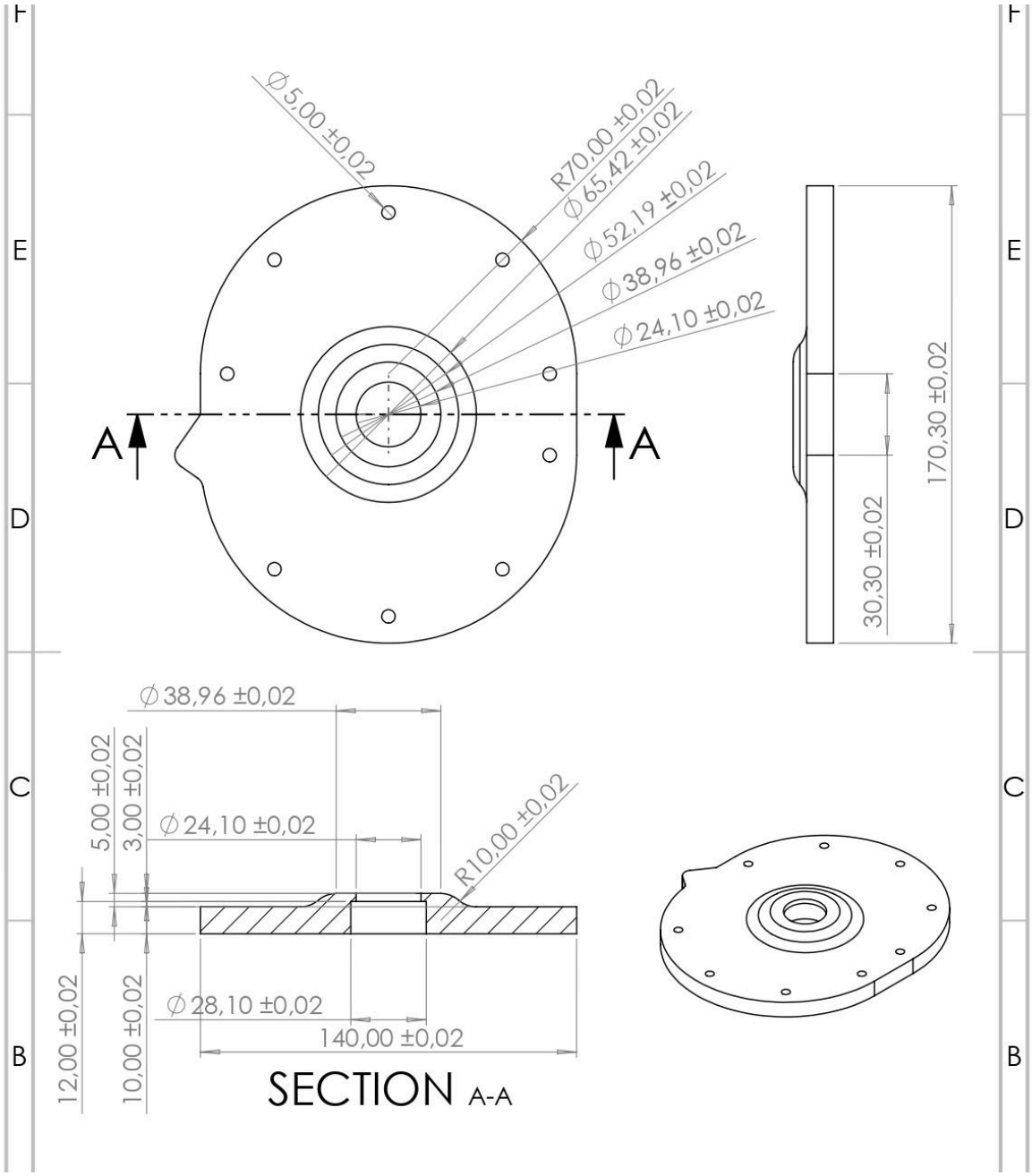

Figure 38. 3D printed Wankel Engine housing cap drawing

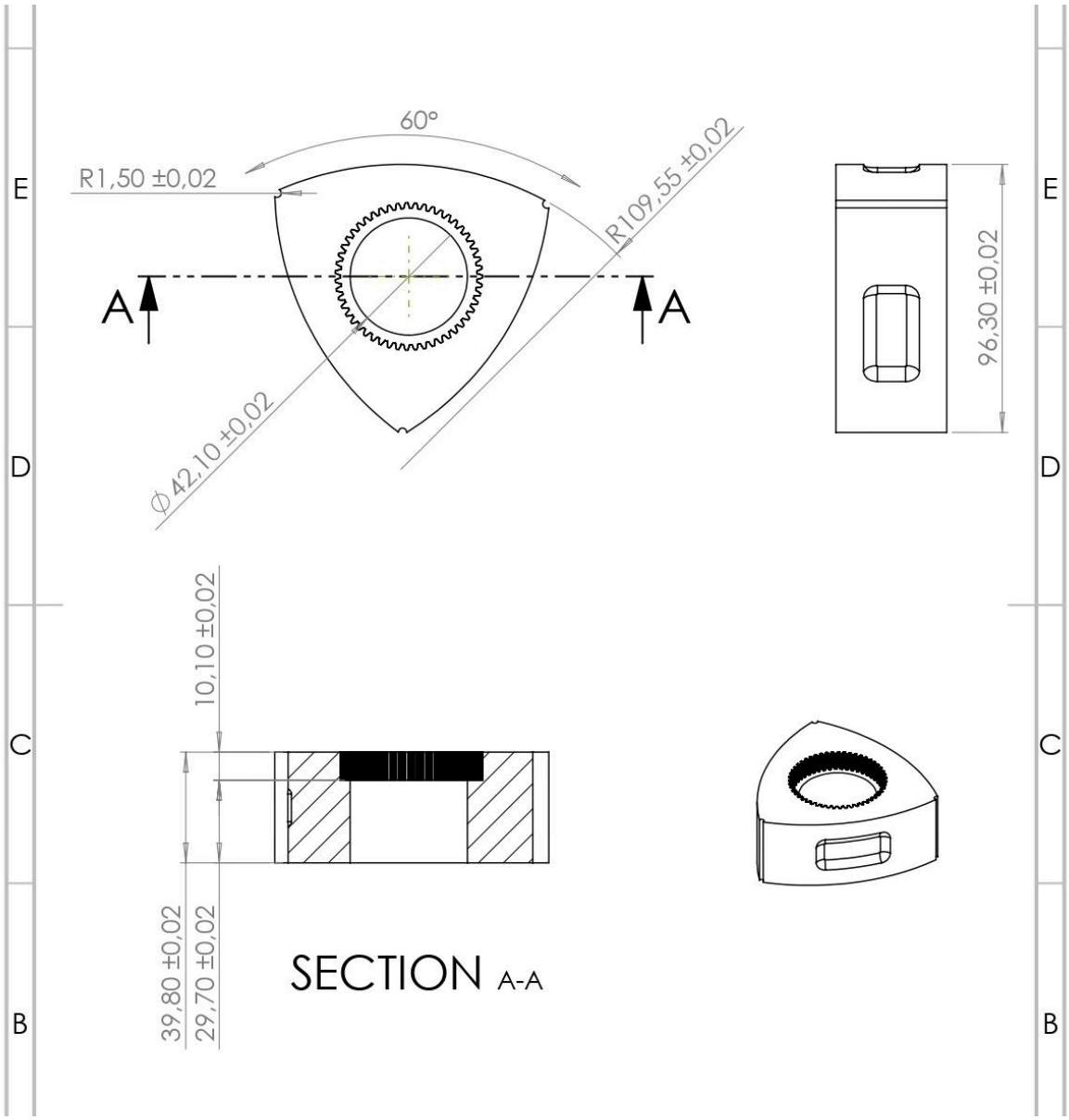

Figure 39. 3D printed Wankel Engine rotor drawing

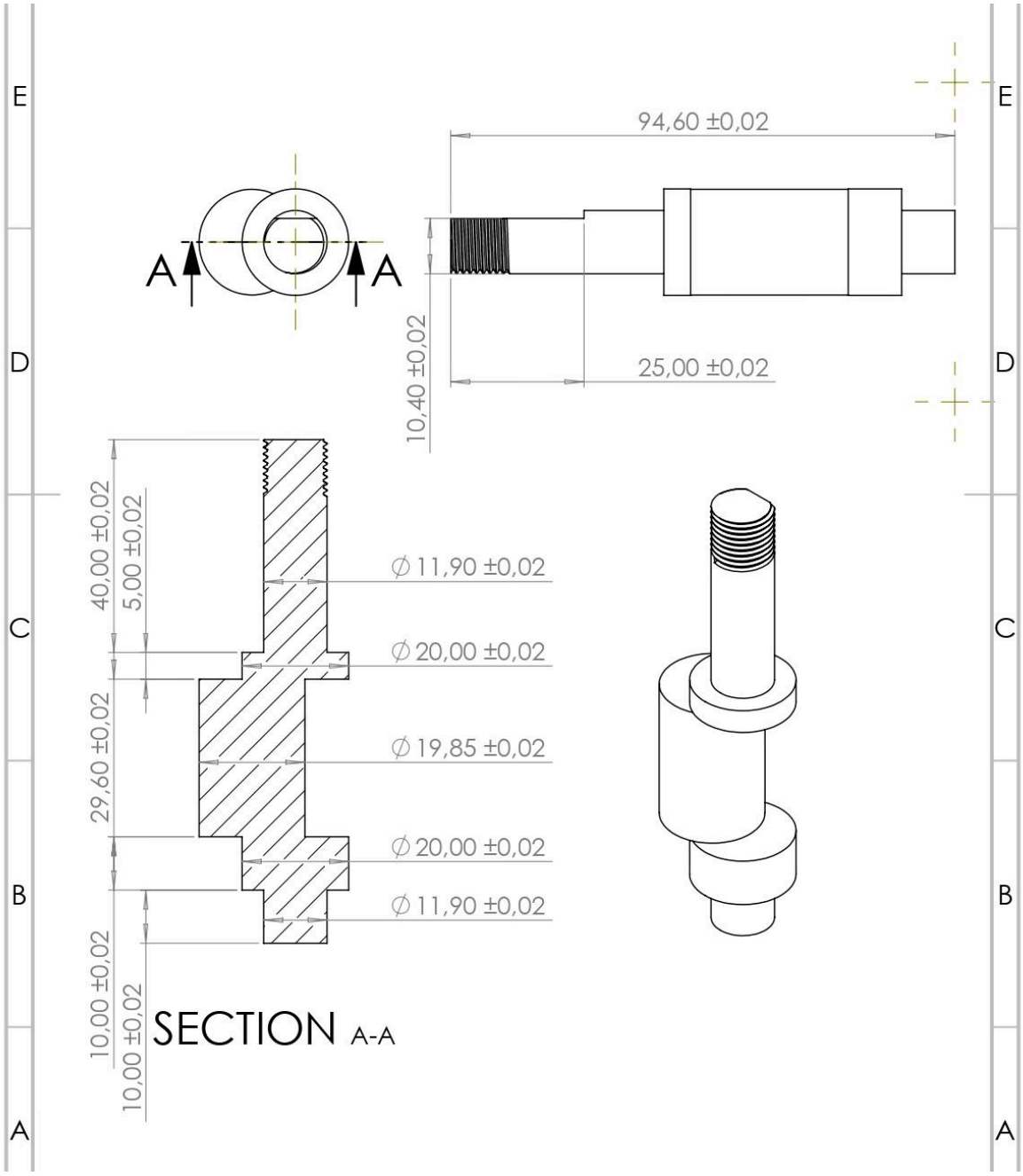

Figure 40. 3D printed Wankel Engine shaft drawing

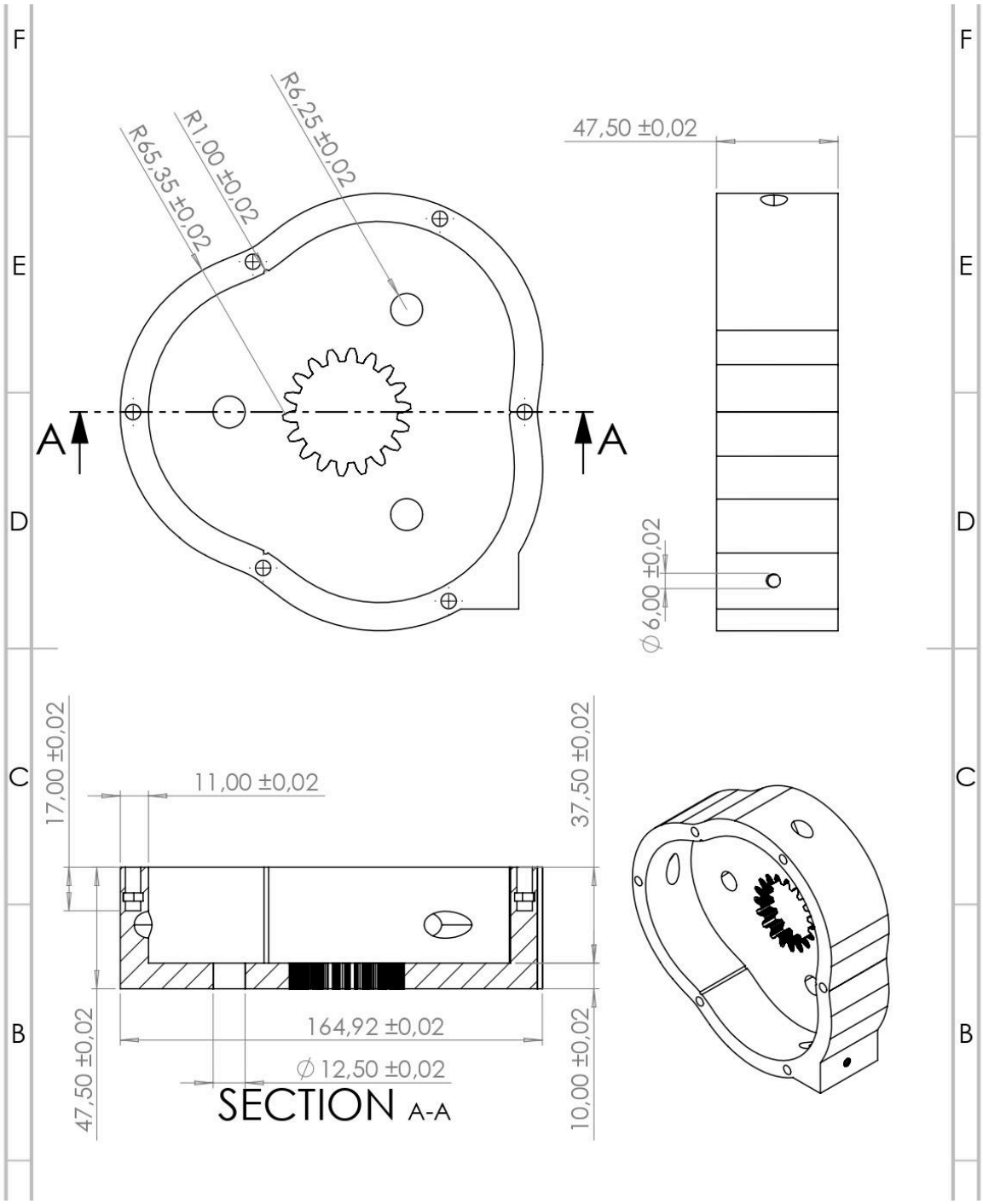

Figure 41. 3D printed LiquidPiston Engine housing drawing

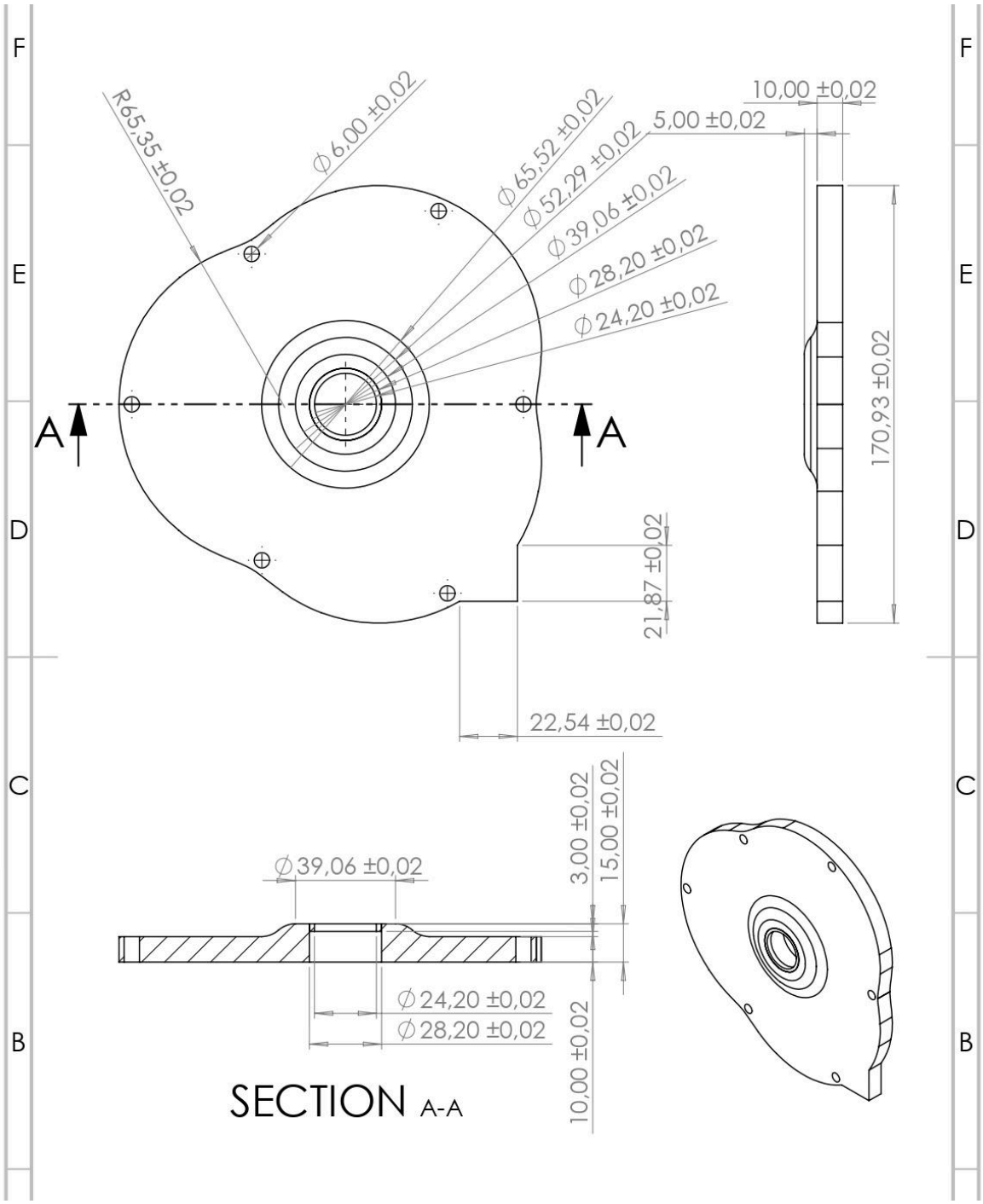

Figure 42. 3D printed LiquidPiston Engine housing cap drawing

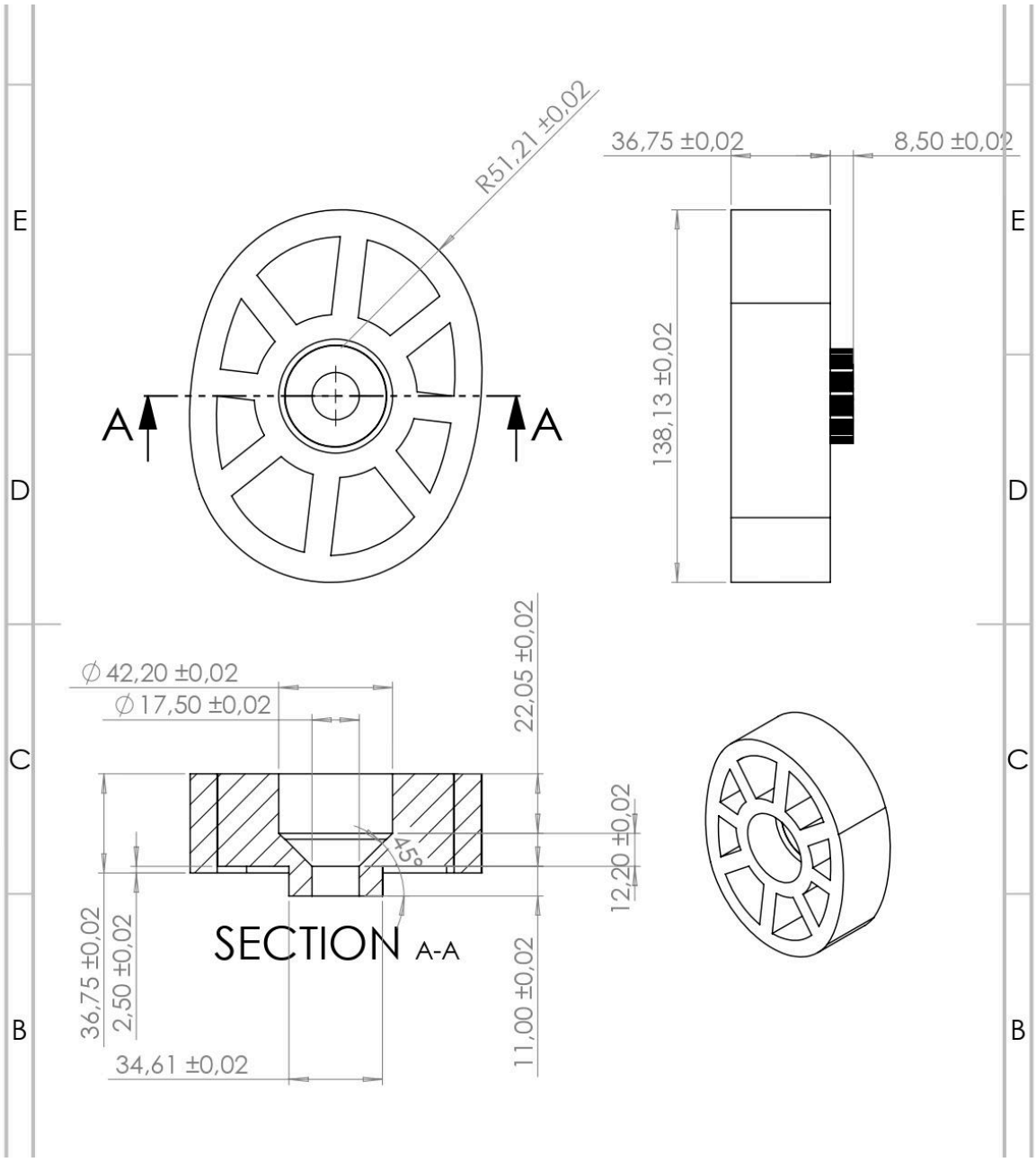

Figure 43. 3D printed LiquidPiston Engine rotor drawing

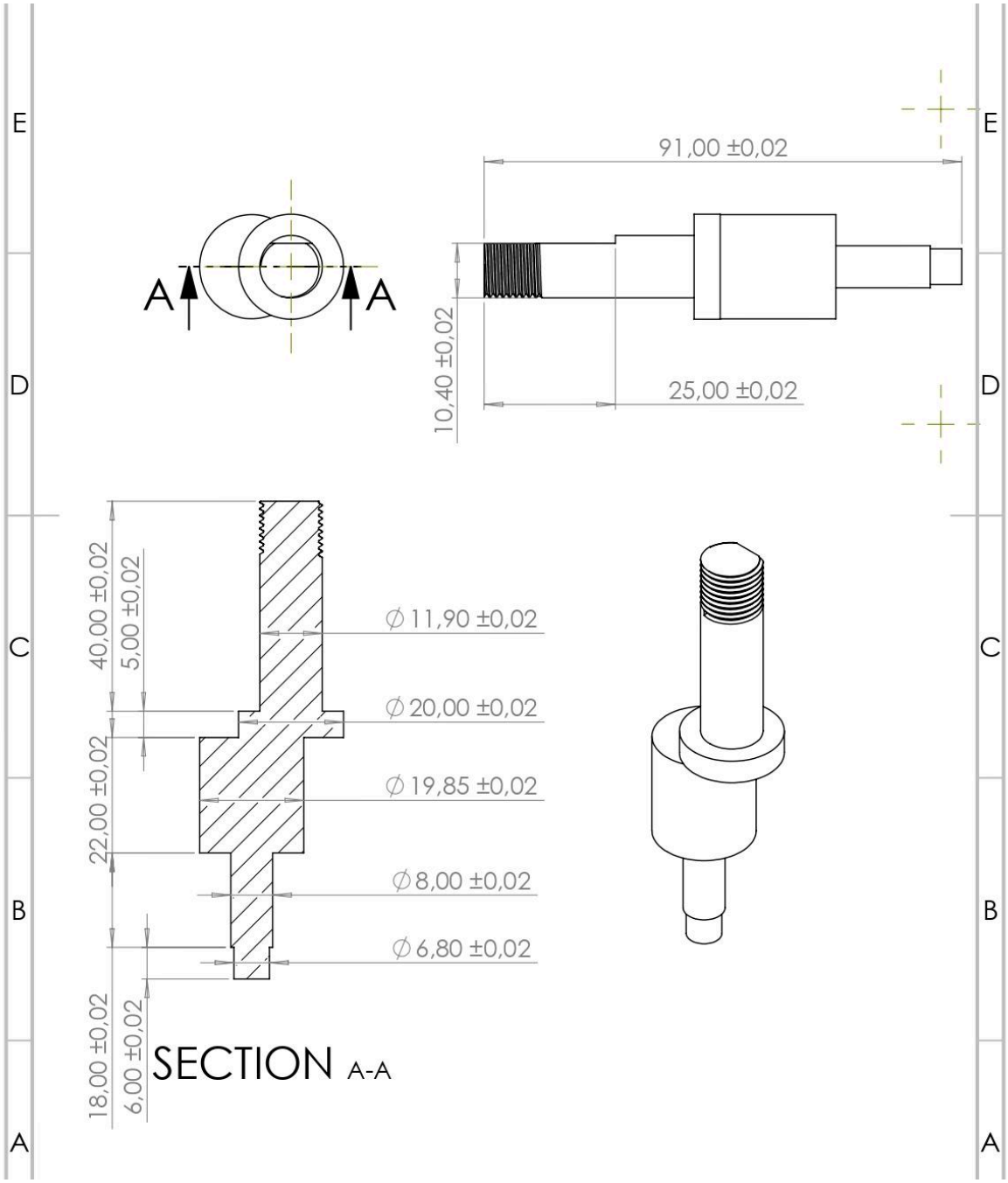

Figure 44. 3D printed LiquidPiston Engine shaft drawing

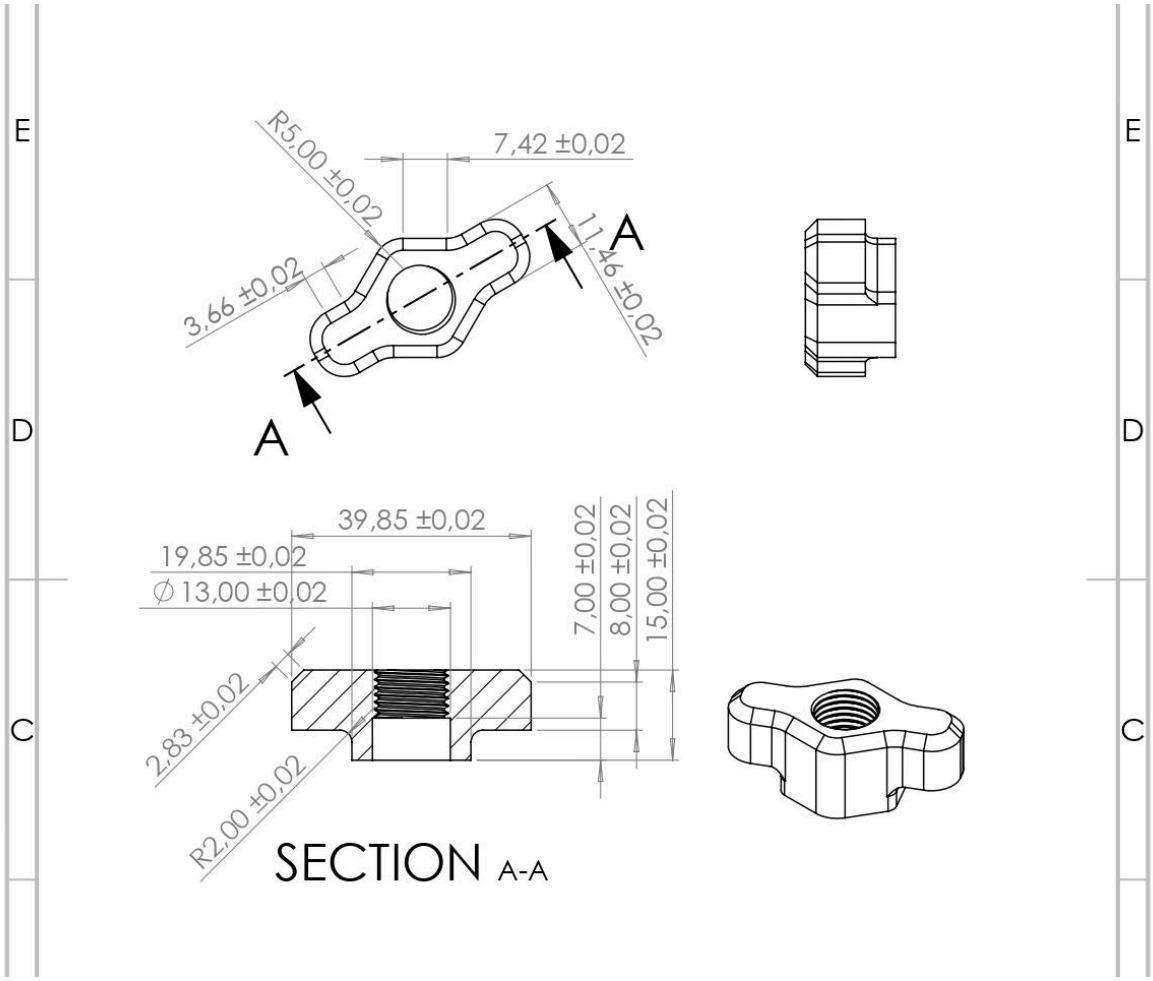

Figure 45. 3D printed Shaft nut drawing

Appendix B. Arduino Code

```
C/C++
#include <Arduino.h>

#define SENSOR_PIN         2       // tach signal → D2 (INT0)
#define TIMEOUT_MS       2000UL    // if no pulse for 2 s → RPM = 0
#define REPORT_INTERVAL_MS 100UL   // 10 Hz reporting
#define BUF_SIZE            8     // median over last 8 intervals

// forward-declare for ISR
class Tachometer;
Tachometer* tach;

class Tachometer {
public:
  Tachometer(byte pin,
             unsigned int ppr = 2,
             unsigned long dbUs = 5000UL)
    : sensorPin(pin),
      pulsesPerRev(ppr),
      debounceUs(dbUs),
      idx(0),
      lastMicros(0),
      lastValidMillis(0)
  {
    for (uint8_t i = 0; i < BUF_SIZE; i++) buf[i] = 0;
  }

  void begin() {
    pinMode(sensorPin, INPUT_PULLUP);
    attachInterrupt(digitalPinToInterrupt(sensorPin),
                    isr, RISING);
  }

  // call in loop()
  float getRPM() {
    // zero-speed detection
    if (millis() - lastValidMillis > TIMEOUT_MS)
      return 0.0f;

    // copy buffer atomically
    unsigned long tmp[BUF_SIZE];
    noInterrupts();
      for (uint8_t i = 0; i < BUF_SIZE; i++)
```

```
        tmp[i] = buf[i];
    interrupts();

    // insertion-sort tmp[]
    for (uint8_t i = 1; i < BUF_SIZE; i++) {
      unsigned long v = tmp[i];
      int8_t j = i - 1;
      while (j >= 0 && tmp[j] > v) {
        tmp[j + 1] = tmp[j];
        j--;
      }
      tmp[j + 1] = v;
    }
    unsigned long medianDt = tmp[BUF_SIZE/2];

    // RPM = 60e6 µs per minute / (medianDt * pulsesPerRev)
    return 60000000.0f / (medianDt * pulsesPerRev);
  }

  // serial tune helpers
  unsigned long getDebounce()       const { return debounceUs; }
  void setDebounce(unsigned long db)       { debounceUs = db; }
  unsigned int  getPulsesPerRev()   const { return pulsesPerRev; }
  void setPulsesPerRev(unsigned int p)    { pulsesPerRev = p; }

private:
  byte            sensorPin;
  unsigned int    pulsesPerRev;
  volatile unsigned long debounceUs;
  volatile unsigned long buf[BUF_SIZE];
  volatile uint8_t idx;
  volatile unsigned long lastMicros;
  volatile unsigned long lastValidMillis;

  // ISR wrapper
  static void isr() {
    tach->handlePulse();
  }

  // runs in interrupt context
  void handlePulse() {
    unsigned long now = micros();
    unsigned long dt  = now - lastMicros;
    lastMicros = now;

    // software-debounce
```

```
    if (dt < debounceUs) return;

    buf[idx] = dt;
    idx = (idx + 1) % BUF_SIZE;

    lastValidMillis = millis();
  }
};

void setup() {
  Serial.begin(9600);
  while (!Serial) {}  // wait for USB Serial (Leonardo, etc)

  // ANSI clear-screen
  Serial.write(0x1B); Serial.print("[2J");
  Serial.write(0x1B); Serial.print("[H");
  Serial.println("=== RPM Monitor ===");
  Serial.println("U/D = debounce ±1 ms, P/O = pulsesPerRev ±1");

  tach = new Tachometer(SENSOR_PIN);
  tach->begin();
}

unsigned long lastReport = 0;

void loop() {
  // -- serial tuning --
  if (Serial.available()) {
    char c = Serial.read();
    if (c == 'u') {
      tach->setDebounce(tach->getDebounce() + 1000UL);
      Serial.print("Debounce_us = ");
      Serial.println(tach->getDebounce());
    }
    else if (c == 'd') {
      unsigned long db = tach->getDebounce();
      db = (db > 1000UL ? db - 1000UL : 0UL);
      tach->setDebounce(db);
      Serial.print("Debounce_us = ");
      Serial.println(tach->getDebounce());
    }
    else if (c == 'p') {
      tach->setPulsesPerRev(tach->getPulsesPerRev() + 1);
      Serial.print("PulsesPerRev = ");
      Serial.println(tach->getPulsesPerRev());
    }
```

```
    else if (c == 'o') {
      unsigned int p = tach->getPulsesPerRev();
      p = (p > 1 ? p - 1 : 1);
      tach->setPulsesPerRev(p);
      Serial.print("PulsesPerRev = ");
      Serial.println(tach->getPulsesPerRev());
    }
  }

  // -- fixed-rate reporting --
  if (millis() - lastReport >= REPORT_INTERVAL_MS) {
    lastReport = millis();
    float rpm = tach->getRPM();
    Serial.print("RPM: ");
    Serial.println(rpm, 1);
  }
}
```